TURBULENCE MODELS AND PLANE LAYER DYNAMOS

C.A. Jones
Department of Mathematical Sciences
University of Exeter, Exeter EX4 4QE, UK

P.H. Roberts
Institute of Geophysics and Planetary Physics
University of California, Los Angeles, CA 90095, USA

The parameter ranges in which naturally-occurring dynamos operate lie far beyond those that are numerically accessible. Small-scale motions that significantly influence the dynamo mechanism cannot be numerically resolved. Two approximate ways that have been suggested for incorporating these "subgrid scales" are investigated here: the addition of hyperdiffusion and the application of the LANS-alpha theory. These proposals were tested by comparing their consequences, not only for marginal convection but also for finite amplitude dynamos, with corresponding "exact" results . Plane layer models were studied because of their numerical advantages.

Both approximate theories raise the differential order of the governing equation so that additional boundary conditions are required. Physical considerations reduce the options but arbitrariness remains. Our choice was the simplest and made it possible to preserve the turbulent character of the solutions while increasing the time step by a factor of about 10, compared with that required by the exact solution at the same spatial resolution. It was found that, for optimal results, the hyperdiffusivities for velocity, momentum and magnetic field should be equal. In the case of the LANS-alpha approximation, a further choice of boundary conditions was investigated. In this model, alpha represents the rms fluid displacement from the mean turbulent motion, both of which vanish at the no-slip boundaries. Analysis of the resulting depression of alpha motivated the alternative conditions that led to even more satisfactory solutions. The question of the best choice of boundary conditions remains open, but is a prime target for future research that uses these methods.

1. Introduction

Substantial progress has been made in modelling the geodynamo in recent years, with Earthlike magnetic fields emerging from convection-driven simulations of the liquid outer core of the Earth. These models are based on self-consistent numerical solutions of the Navier-Stokes equation and the magnetic induction equation. This work has been reviewed recently by Kono and Roberts (2002) and from a more observational standpoint by Dormy *et al.* (2000). There is, however, a disturbing feature of these simulations; the dimensionless parameters used are very different from those suggested by the molecular diffusion constants relevant to the outer core. For example, the Ekman number $E = \nu/2\Omega d^2$, where ν is the kinematic viscosity, Ω is the Earth's angular velocity, and d is the outer core radius, is about 10^{-15} in the core, but values of order 10^{-4} are typically used in simulations. Similarly, the heat flux Rayleigh number, which is defined as $Ra = Fg\bar{\alpha}d^2/2\Omega\kappa^2\rho c_p$ where F is the heat flux per unit area emerging from the core, g is gravity, $\bar{\alpha}$ is the thermal expansion coefficient, κ is the thermal diffusivity, ρ is the density and c_p is the specific heat, is approximately 10^{15}, whereas values between of order $10^2 - 10^3$ are used in simulations. The Prandtl number $P_r = \nu/\kappa$ in the core is about 0.1, and the magnetic Prandtl number $P_m = \nu/\eta$ is estimated to be about 10^{-6}, where η is the magnetic diffusivity, but in simulations O(1) values of P_m are assumed. Indeed, no successful simulations have been performed with $q = P_m/P_r$ small; even using such modest values as $q \sim 0.1$ is currently out of reach (Christensen *et al.* 1999). It is therefore rather surprising that geodynamo simulations give results that apparently agree well with observation.

The scaling arguments of Starchenko and Jones (2002) shed some light on this paradox. They argue that the MAC balance is the relevant one for the core, that is Coriolis, pressure, buoyancy and Lorentz forces are all of similar magnitudes. In the limit of small diffusion, this leads to an estimate for the typical velocity $u_* \sim (g\alpha F/2\Omega\rho c_p)^{1/2}$ that is independent of all diffusivities, and has the right order of magnitude when compared with the velocities inferred from the secular variation. A similar criterion exists for compositional convection. In consequence, provided a geodynamo simulation uses

the right heat flux, and provided it is in the correct asymptotic MAC regime, a reasonable magnitude for the velocity will emerge even if the thermal and viscous diffusivities are completely incorrect.

Using a plane layer dynamo model, Rotvig and Jones (2002) showed that at moderate Rayleigh number the MAC regime (as evidenced by the progressive satisfying of Taylor's (1963) constraint) is attained for $10^{-4} < E < 10^{-5}$ at moderate Rayleigh number. This suggests that current spherical geometry geodynamo models are on the verge of entering the MAC regime, but to get fully into this regime in spherical geometry is still computationally very challenging. Even if this difficulty is overcome, a further hurdle lies ahead, that raised by the large Rayleigh number (low thermal diffusivity) of core flow. The Earth's core and all experimental dynamos are liquid metal systems in which the magnetic diffusity is much greater than the thermal diffusivity. This is currently a very difficult numerical regime for dynamo codes, and so the issue of whether the MAC balance regime is achieved in the limit of small κ is still largely unexplored.

A wide variety of numerical methods have been employed to attack the dynamo problem, the pseudo-spectral method, finite differences and finite elements all being used. Spherical harmonic expansion in the ϑ and ϕ directions, (r, ϑ, ϕ) being spherical polar coordinates, and finite differences in r are a popular choice. All these methods have a common difficulty, which is intrinsic to the problem, that of the appearance of waves on many different timescales. This is a consequence of the large number of different forces involved in the dynamical balance. Unfortunately, this obstacle has yet to be removed, so that little further progress has been made since the initial successes in the mid nineties. The aim of this article is to analyse the difficulties and to identify promising directions for future simulations.

Since the difficulties are clearly associated with the presence of small diffusion terms, it is natural to focus on the modelling of these processes in the Earth's core. It is of course true that similar problems occur in all modelling of problems where the diffusive processes are small in dimensionless terms such as, for example, the turbulent flow in wind-tunnels. Nevertheless, there are very particular difficulties which arise in the dynamo problem over and above those of high Reynolds number non-magnetic, non-rotating flows. It is arguable that to represent the geodynamo adequately, we need to be able to resolve scales on which the magnetic Reynolds number is around unity. Since the large scale magnetic Reynolds number in the core is only a few hundred, this would not appear to be an impossible challenge, but numerical difficulties have so far prevented this goal from being attained.

The difficulties found in spherical systems appear to be similar to those found in plane layer geometry, but planar models are much better suited to experimentation, as the numerical codes are much simpler. These codes also run faster because of the availability of practical fast Fourier transforms in all three spatial dimensions. Plane layer geometry therefore provides an excellent test bed for new numerical schemes, and for evaluating ideas of subgrid scale modelling.

We believe that the difficulties are intrinsic to the dynamo problem and arise from the nature of the wave modes inside the core. It is therefore unlikely that the problem can be avoided by using a different numerical method, though of course some methods are more stable than others, and some are more efficient than others. We adopt the view that the equations themselves have to be modified to take into account the particular nature of the dynamics of the core. One way forward is to introduce hyperdiffusion to overcome the numerical difficulties. Another is to attempt to model the small scale motions, and so add further terms to the equations. The traditional "eddy" viscosity' model can be viewed as an example of this approach, though here only the magnitude of the diffusion terms are enhanced, the form of the diffusion operator still being the divergence of a gradient. Further modifications, such as the Smagorinsky method, in which the eddy viscosity is taken to be dependent on the local properties of the solution (e.g., diffusion is assumed to be enhanced by turbulence in regions of strong shear) are also possible, see for example Buffett (2003). The LANS α-model (Lagrangian averaged Navier-Stokes α-model) is a more radical step in this direction, because here the form of the diffusion process is assumed to change as a result of the turbulence, so that fourth order "hyperdiffusive" terms enter the equations. There is therefore a link between the addition of these terms and the attempts to model the subgrid scale processes.

There are however, two rather different philosophies possible here, which can affect the way in which the theory is developed. On the one hand, the problem of the subgrid scales can be attacked by purely numerical methods. Prominent amongst these is the introduction of hyperdiffusion. This

was done by Glatzmaier and Roberts (1995, 1997) and by Kuang and Bloxham (1999) essentially as a numerical method to help stabilise the equations. No physical argument was advanced to justify the form of the hyperdiffusion used. This is a reasonable approach if it can be shown that the form of the low order large scale modes is not significantly affected by the hyperdiffusion. After all, numerical methods invariably involve truncation of modes (or equivalently limitations of the mesh size), so that there is essentially nothing new in this approach. Unfortunately, the analysis of Zhang and Jones (1997) and Zhang *et al.* (1998) showed that hyperdiffusion has a significant effect on the onset of convection, and Grote *et al.* (2000) showed that the anisotropic hyperdiffusion used by Glatzmaier and Roberts and Kuang and Bloxham has a substantial effect on the character of the solutions. One of the aims of the present work is to see whether these objections can be overcome by the use of isotropic hyperdiffusion, and to determine, by comparing the results with non-hyperdiffusive solutions, whether hyperdiffusivity is a useful numerical tool. Finite difference CFD schemes commonly employ some form of shock-capturing algorithm, which smooths out regions in which very rapid variations of the dependent variables occur. Hyperdiffusion can play a similar role in pseudo-spectral codes. It follows from this approach that the aim should be to minimise the effects of the hyperdiffusive terms wherever possible, especially in the choice of boundary conditions. When following this philosophy, we also want to gain maximum numerical stabilisation, and hence allow larger timesteps, while maintaining a minimum of added hyperdiffusion.

If, on the other hand, the additional terms are motivated by physical models of the subgrid scale processes, we might hope that the results are more realistic than those of a simple truncation of the equations at a given wavenumber. In this case, we are not constrained by having to produce optimal results from the standard equations. For example, it is possible that energy can be injected on small scales and then, instead of being dissipated by viscosity, it may flow into the large scales. This is known as "back-scatter". If it is an active process, the idea of merely enhancing dissipation through hyperdiffusion may not be the best option. Also, if the form of the subgrid scale terms has a plausible physical basis, it may be acceptable to study systems that can run only if the timestep is comparatively small, i.e., numerical stability is not necessarily the paramount consideration. The test of whether the subgrid scale models are performing well is then through comparison of low-resolution models that include subgrid scale modelling with high resolution runs of the "raw" equations.

The methods considered here are by no means the only possible ways forward, and a number of other directions are currently being explored. One such is the similarity method, where the behaviour on the smallest resolved scales in the computation are analysed and it is assumed that the unresolved scales behave in a similar manner (e.g., Buffett, 2003). Yet another approach is the shell model method, which assumes the behaviour on the smallest scales is isotropic and self-similar, and can therefore be adequately represented by blocking together the large Fourier wavenumber modes into shells in Fourier space (e.g., Frick *et al.*, 2002).

2. Background to the LANS $\alpha-$models

A detailed description of the reasoning that provided motivation for the $\alpha-$equations would occupy more space than could be justified; only a sketch is given here. See also Montgomery and Pouquet (2002).

The basic idea may be attributed to Andrews and McIntyre (1978a,b), and is most easily illustrated for a compressible, non-rotating, non–magnetic, inviscid, isentropic fluid moving adiabatically, what is often called a "barotropic fluid". In turbulent flow, the paths $\mathbf{X}(\mathbf{x}_0, t)$ of fluid elements from an initial state $\mathbf{x}_0$ scatter about a mean trajectory $\mathbf{x}(\mathbf{x}_0, t)$, the separation between them, $\boldsymbol{\xi} = \mathbf{X} - \mathbf{x}$, not being necessarily small. Similarly, the difference $\mathbf{u}^\ell = D_t\boldsymbol{\xi}$ between the velocity $\mathbf{u}^*(\mathbf{X}, t)$ of the fluid element and the contemporaneous velocity $\overline{\mathbf{u}}^L(\mathbf{x}, t)$ of the corresponding point on the reference trajectory is not small in general. Here $D_t = \partial_t + \overline{\mathbf{u}}^L\boldsymbol{\cdot\nabla}$, where $\partial_t = \partial/\partial t$ for fixed $\mathbf{x}$ and $\nabla_i = \partial/\partial x_i$ for fixed t. Lagrangian averages such as $\overline{\mathbf{u}}^L$ are defined as averages for fixed $\mathbf{x}_0$ or equivalently by

$$\overline{\chi(\mathbf{x}, t)}^L = \overline{\chi(\mathbf{X}, t)}, \tag{2.1}$$

i.e., $\overline{\chi}^L$ is the ensemble average of $\chi(\mathbf{X}, t)$ referred back to $\mathbf{x}$. The technique of making such transformations was initiated by Eckart (1963) and developed further by Soward (1972). It is worth observing that $\rho(\mathbf{x}, t)$ for the reference orbit is defined as $\mathcal{J}\rho^*(\mathbf{X}, t)$, where $\mathcal{J} = \partial(X_1, X_2, X_3)/\partial(x_1, x_2, x_3)$ is

the Jacobian of the transformation $\mathbf{X} \to \mathbf{x}$; it follows that $\rho^*(\mathbf{X})d^3X = \rho(\mathbf{x})d^3x$. For the transformed equation of motion, see (5.4) of Soward (1972). The averaged form of the transformed equation was given by Andrews and McIntyre (1978a) and called by them "the Generalized Lagrangian Mean equation" (or "GLM equation"); see their (3.8). This was recovered by Holm from the Lagrange-averaged Lagrangian by an application of Hamilton's principle; e.g., see Holm (2002).

The application of GLM theory to practical situations assumes that a large eddy simulation (LES) gives the mean trajectory about which the subgrid scales (SGS) provide the scatter. The better the resolution of the LES, the smaller the scatter, and one can imagine that in many circumstances of interest the scatter is so small that the evolution of $\boldsymbol{\xi}$ is well represented by a linear equation, and also that only terms up to quadratic order are needed in the lagrangian ℓ to recognize the effect of the SGS on the LES:

$$\ell = \ell_0 + \ell' + \tfrac{1}{2}\ell'' \tag{2.2}$$

where ℓ_0, ℓ' and ℓ'' are of order ξ^0, ξ and ξ^2 respectively. Holm (2002, §4.2) obtained

$$\begin{aligned} \ell_0 &= \int \overline{\rho}(\tfrac{1}{2}\overline{u}^2 - \overline{U})\, d^3x, \qquad \ell' = \int [\rho'(\tfrac{1}{2}\overline{u}^2 - \overline{W}) + \overline{\rho}\mathbf{u}'\cdot\overline{\mathbf{u}}]\, d^3x \\ \ell'' &= \int [\overline{\rho}u'^2 + 2\rho'\mathbf{u}'\cdot\overline{\mathbf{u}} - \overline{c}^2\rho'^2/\overline{\rho}]\, d^3x \end{aligned} \tag{2.3}$$

where U is the internal energy, $W = U + P/\rho$ is the enthalpy (both per unit mass) and c is the sound speed; for a barotropic fluid all these, and the pressure P, depend on ρ alone. Clearly $\overline{\ell'} = 0$ and, with the help of

$$\mathbf{u}' = \partial_t\boldsymbol{\xi} + \overline{\mathbf{u}}\cdot\boldsymbol{\nabla}\boldsymbol{\xi} - \boldsymbol{\xi}\cdot\boldsymbol{\nabla}\overline{\mathbf{u}}, \qquad \rho' = -\boldsymbol{\nabla}\cdot(\overline{\rho}\,\boldsymbol{\xi}), \tag{2.4, 2.5}$$

Holm (2002) argued that

$$\ell'' = \int [\partial_t\boldsymbol{\xi}\cdot\overleftrightarrow{\mathbf{A}}\cdot\partial_t\boldsymbol{\xi} + \partial_t\boldsymbol{\xi}\cdot\overleftrightarrow{\mathbf{B}}\cdot\boldsymbol{\xi} + \boldsymbol{\xi}\cdot\overleftrightarrow{\mathbf{C}}\cdot\boldsymbol{\xi}]\, d^3x, \tag{2.6}$$

where the tensors $\overleftrightarrow{\mathbf{A}}$, $\overleftrightarrow{\mathbf{B}}$ and $\overleftrightarrow{\mathbf{C}}$ depend only on $\overline{\mathbf{u}}$, $\overline{\rho}$ and their gradients. Clearly $\overline{\ell''}$ involves statistical averages of quadratic products involving $\boldsymbol{\xi}$ and/or $\partial_t\boldsymbol{\xi}$. To make progress it is necessary to obtain information about these. Once this has been done, an application of Hamilton's principle to $\overline{\ell}$ will provide an equation of motion governing the LES with the mean effects of the SGS built in.

Two possible ways of closing the theory may be attempted. The first is to solve the linear equation governing the evolution of $\boldsymbol{\xi}$ in terms of $\overline{\mathbf{u}}$ and $\overline{\rho}$. This was the approach of Gjaja and Holm (1996), in which the $\boldsymbol{\xi}$ equation was attacked by WKBJ methods. Alternatively the new equation for $\overline{\mathbf{u}}$ could be solved in conjunction with that governing $\boldsymbol{\xi}$ and the necessary quadratic averages obtained from the latter as the integration proceeded. In either case the theory has been closed in an approximate, though physically-consistent, way.

A second, and much simpler, procedure is to make an *ad hoc* assumption about the unknown quadratic moments. In §5 of his paper, Holm (2002) lists four possible Ansätze, which he names in honour of G.I. Taylor. The first ansatz is the simplest and leads quickly to the $\alpha-$model. Equation (2.4) is separated into two parts:

$$\partial_t\boldsymbol{\xi} + \overline{\mathbf{u}}\cdot\boldsymbol{\nabla}\boldsymbol{\xi} = 0, \qquad \mathbf{u}' = -\boldsymbol{\xi}\cdot\boldsymbol{\nabla}\overline{\mathbf{u}}. \tag{2.7, 2.8}$$

Since $\overline{\mathbf{u}}$ and $\overline{\mathbf{u}}^L$ differ only at quadratic order in $\boldsymbol{\xi}$, (2.7) gives $\mathbf{u}^\ell = 0$, to leading order. It also follows from (2.7) that

$$(\partial_t + \overline{\mathbf{u}}\cdot\boldsymbol{\nabla})\overline{\xi_i\xi_j} = 0, \tag{2.9}$$

so that $\overline{\xi_i\xi_j}$ is invariant following the mean motion. The easiest and most natural assumptions are that it is isotropic and homogeneous:

$$\overline{\xi_i\xi_j} = \alpha^2\delta_{ij}, \qquad \alpha = \text{constant}. \tag{2.10}$$

This defines the $\alpha-$model. It is also found that (2.6) simplifies considerably to give

$$\overline{\ell} = \int \overline{\rho}[\tfrac{1}{2}(\overline{u}^2 + \alpha^2(\boldsymbol{\nabla}\overline{\mathbf{u}})^2) + \frac{\alpha^2}{2\overline{\rho}}\boldsymbol{\nabla}|\overline{\mathbf{u}}|^2 \cdot \boldsymbol{\nabla}\overline{\rho} - \frac{\alpha^2\overline{c}^2}{2\overline{\rho}^2}|\boldsymbol{\nabla}\overline{\rho}|^2 - U(\overline{\rho})]\, d^3x. \tag{2.11}$$

Hamilton's principle then gives

$$(\partial_t + \overline{\mathbf{u}}\cdot\boldsymbol{\nabla})\mathbf{u} + (\boldsymbol{\nabla}\overline{\mathbf{u}})\cdot\mathbf{u} = -\boldsymbol{\nabla}\Pi \tag{2.12}$$

where

$$\mathbf{u} = \overline{\mathbf{u}} - \alpha^2[\nabla^2\overline{\mathbf{u}} + \frac{1}{\overline{\rho}}(\boldsymbol{\nabla}\overline{\rho}\cdot\boldsymbol{\nabla})\overline{\mathbf{u}} + \frac{1}{\overline{\rho}}\overline{\mathbf{u}}\nabla^2\overline{\rho}], \tag{2.13}$$

$$-\Pi = (1-\alpha^2\nabla^2)(\tfrac{1}{2}\overline{u}^2 - \overline{W}) + \tfrac{1}{2}\alpha^2(\boldsymbol{\nabla}\overline{\mathbf{u}})^2 - \tfrac{1}{2}\alpha^2(\boldsymbol{\nabla}\overline{\rho})^2(\frac{2\overline{c}}{\overline{\rho}}\frac{d\overline{c}}{d\overline{\rho}} - \frac{\overline{c}^2}{\overline{\rho}^2}). \tag{2.14}$$

In the remainder of this paper, we shall assume that the fluid is incompressible. To obtain the equations that then replace (2.12)–(2.14), the argument just given must be modified by introducing the constraint of constant density into the Lagrangian with a Lagrance multiplier that is interpreted as a "reduced pressure" Π. Alternatively, by setting $\overline{\rho}$ =constant in (2.12)–(2.14), we again obtain (2.12), but with a different (and irrelevant) Π and with

$$\mathbf{u} = (1-\alpha^2\nabla^2)\overline{\mathbf{u}}. \tag{2.15}$$

Equation (2.12) has a very attractive property (that is however not significant for the topic of this paper where the inertial terms are neglected). It preserves Kelvin's theorem in the sense that the circulation of $\mathbf{u}$ round a closed contour carried by the mean motion $\overline{\mathbf{u}}$ is conserved.

The effects of viscous friction are ignored in (2.12). If the fluid is incompressible, the equation governing $\mathbf{u}^*(\mathbf{X})$ would include a term $\nu\nabla^2_{\mathbf{X}}\mathbf{u}^*$, where ν is a constant kinematic viscosity. The transformation $\mathbf{X} \to \mathbf{x}$ complicates this term; see the analogous expression given by Soward (1972) for ohmic diffusion in the induction equation governing the magnetic field $\mathbf{B}$. To avoid such complications, the effects of which are not necessarily serious, it is customary to recognize viscosity by adding a term such as $\nu\nabla^2\mathbf{u}$ to the right-hand side of (2.12).

In what follows, $\mathbf{u}^*$ will be called "the unfiltered velocity" and will usually be written simply as $\mathbf{u}$ while $\overline{\mathbf{u}}^L$ will be termed "the filtered velocity" and written as $\overline{\mathbf{u}}$.

3. Model Description and Governing Equations

We consider a conducting fluid layer confined between horizontal boundaries at $z = \pm\frac{1}{2}d$ as in Jones and Roberts (2000). We seek solutions in a "box" that are periodic in both the x–direction (period $2\pi d/k_x$) and the y–direction (period $2\pi d/k_y$).

The magnetic diffusivity is η, the thermal diffusivity is κ and the kinematic viscosity is ν. The layer is rotating at angular velocity Ω about the upward vertical axis, Oz. The coefficient of thermal expansion is $\bar{\alpha}$ and the temperature difference across the layer is βd.

In the Earth's core, the inertial terms in the momentum equation are small compared with the Coriolis term (i.e., the Rossby number is small) and are often neglected, as in the high Prandtl number limit ($\nu/\kappa \to \infty$) considered here. Taking the length scale as the layer-depth d, the timescale as the magnetic diffusion time d^2/η, the magnetic field unit as $(2\Omega\rho\mu\eta)^{1/2}$ (where ρ is the fluid density and μ the permeability) and the temperature unit as βd, the governing equations are

$$\hat{\mathbf{z}}\times\mathbf{u} = -\boldsymbol{\nabla}p + \mathbf{j}\times\mathbf{B} + qRa\theta\hat{\mathbf{z}} + E\nabla^2\mathbf{u}, \tag{3.1}$$

$$\partial_t\mathbf{B} = \boldsymbol{\nabla}\times(\mathbf{u}\times\mathbf{B}) + \nabla^2\mathbf{B}, \tag{3.2}$$

$$\partial_t\theta + \mathbf{u}\cdot\boldsymbol{\nabla}\theta = q\nabla^2\theta + \mathbf{u}\cdot\hat{\mathbf{z}}, \tag{3.3}$$

$$\boldsymbol{\nabla}\cdot\mathbf{B} = 0, \qquad \boldsymbol{\nabla}\cdot\mathbf{u} = 0, \tag{3.4, 3.5}$$

where $\mathbf{B}$ is the magnetic field, θ is the difference between the actual temperature gradient and the static temperature gradient and $\mathbf{j} = \boldsymbol{\nabla}\times\mathbf{B}$ is the current density. The three dimensionless parameters are E, the Ekman number, Ra, the Rayleigh number and q, the diffusivity ratio defined by

$$E = \frac{\nu}{2\Omega d^2}, \qquad Ra = \frac{g\bar{\alpha}\beta d^2}{2\Omega\kappa}, \qquad q = \frac{\kappa}{\eta}. \tag{3.6}$$

The velocity and magnetic field are expanded in toroidal and poloidal components, but in the plane layer geometry horizontally averaged horizontal components must be added explicitly to obtain the complete representation:

$$\mathbf{u} = \boldsymbol{\nabla}\times e\hat{\mathbf{z}} + \boldsymbol{\nabla}\times\boldsymbol{\nabla}\times f\hat{\mathbf{z}} + U_x\hat{\mathbf{x}} + U_y\hat{\mathbf{y}}, \tag{3.7}$$

$$\mathbf{B} = \boldsymbol{\nabla}\times g\hat{\mathbf{z}} + \boldsymbol{\nabla}\times\boldsymbol{\nabla}\times h\hat{\mathbf{z}} + b_x\hat{\mathbf{x}} + b_y\hat{\mathbf{y}}. \tag{3.8}$$

Here U_x and U_y define what we call "the mean velocity", and b_x and b_y define "the mean field"; they are functions of z and t alone.

The scalar equations solved are formed by taking the z-components of the curl and of the curl^2 of equation (3.1) and the z-components of (3.2) and of the curl of (3.2):

$$\nabla_H^2(\partial_z f + E\nabla^2 e) = \hat{\mathbf{z}}\cdot\boldsymbol{\nabla}\times(\mathbf{j}\times\mathbf{B}), \tag{3.9}$$

$$\nabla_H^2(\partial_z e - E\nabla^4 f + qRa\theta) = \hat{\mathbf{z}}\cdot\boldsymbol{\nabla}\times\boldsymbol{\nabla}\times(\mathbf{j}\times\mathbf{B}), \tag{3.10}$$

$$\nabla_H^2(\partial_t - \nabla^2)g = -\hat{\mathbf{z}}\cdot\boldsymbol{\nabla}\times(\mathbf{u}\times\mathbf{B}), \tag{3.11}$$

$$\nabla_H^2(\partial_t - \nabla^2)h = -\hat{\mathbf{z}}\cdot\boldsymbol{\nabla}\times\boldsymbol{\nabla}\times(\mathbf{u}\times\mathbf{B}), \tag{3.12}$$

where ∇_H^2 denotes the horizontal Laplacian. Our fifth scalar equation is (3.3).

These equations must be supplemented by the equations for the horizontally averaged components:

$$-U_y - E\partial_z^2 U_x = \hat{\mathbf{x}}\cdot\langle\mathbf{j}\times\mathbf{B}\rangle, \tag{3.13}$$

$$U_x - E\partial_z^2 U_y = \hat{\mathbf{y}}\cdot\langle\mathbf{j}\times\mathbf{B}\rangle, \tag{3.14}$$

$$(\partial_t - \partial_z^2)b_x = \hat{\mathbf{x}}\cdot\langle\nabla\times(\mathbf{u}\times\mathbf{B})\rangle, \tag{3.15}$$

$$(\partial_t - \partial_z^2)b_y = \hat{\mathbf{y}}\cdot\langle\nabla\times(\mathbf{u}\times\mathbf{B})\rangle, \tag{3.16}$$

where $\langle\ldots\rangle$ denotes the horizontal average

$$\langle f\rangle = \frac{k_x k_y}{4\pi^2}\int f dx dy. \tag{3.17}$$

The choice of boundary conditions is rather important. They divide into two classes, those that are required for (3.3), (3.9) – (3.16) to form a well-posed system, which we call "the large scale boundary conditions", and the additional boundary conditions that must be imposed when the order of the diffusion operators is increased due either to the addition of hyperdiffusion or to the use of subgrid scale filtering. We call these additional boundary conditions "the subgrid scale boundary conditions". We may wish to add terms to the large scale boundary conditions as a result of the filtering, but any such terms should vanish in the limit in which the filter size tends to zero.

For the large scale velocity conditions we take the no-slip velocity boundary conditions,

$$e = f = f' = U_x = U_y = 0 \qquad \text{on} \qquad z = \pm\tfrac{1}{2}, \tag{3.18}$$

where $f' = \partial_z f$. As shown in Jones and Roberts (2000) the use of perfectly conducting boundary conditions can prevent the formation of a mean field $(b_x, b_y, 0)$. We therefore adopt magnetically insulating boundary conditions. The magnetic field outside the fluid layer is then current-free; $j_z = 0$ implies $g = 0$ in the insulators, and $j_x = j_y = 0$ implies $\nabla^2 h = 0$ there. Zero current in the insulators implies that the mean field there, $(b_x, b_y, 0)$, must be constant in z. We could take this constant to be

non-zero, but this would correspond to the problem of dynamo action in an imposed external field, which we do not consider here. We therefore assume the field tends to zero at large distance from the layer, so that in the insulators $b_x = b_y = 0$. Continuity of tangential field then requires

$$g = b_x = b_y = 0 \qquad \text{on} \qquad z = \pm\tfrac{1}{2}, \tag{3.19}$$

and since each component of the potential field h must decay exponentially away from the layer, continuity of h and its vertical derivative implies that

$$h'_{lm} = \mp a\, h_{lm} \qquad \text{on} \qquad z = \pm\tfrac{1}{2}, \tag{3.20}$$

where h_{lm} denotes the Fourier component of h with wavenumber lk_x in the x–direction and mk_y in the y–direction, and which therefore has a total wavenumber of $a = (l^2k_x^2 + m^2k_y^2)^{1/2}$. The temperature condition is

$$\theta = 0 \qquad \text{on} \qquad z = \pm\tfrac{1}{2}. \tag{3.21}$$

The equations are solved by the pseudo-spectral method, a brief description being given in Jones and Roberts (2000). The fields are expanded in Fourier series in x and y, and Chebyshev series in z. The Fourier series are truncated at the N_x and N_y levels, so only harmonics in the range $(-N_x, N_x)$ and $(-N_y, N_y)$ are retained, and $N_z + N_{bc}$ Chebyshev components are retained for each variable, where N_{bc} depends on the number of boundary conditions. We have not imposed any particular symmetry on the solutions. Because the Boussinesq approximation has been adopted and the boundary conditions on the horizontal surfaces are the same, many symmetric solutions exist, but we have explored only the asymmetric solutions which arise naturally if a random initial seed field is used to start the calculation.

With a typical truncation of $N_x = N_y = N_z = 32$, there are of the order of 130,000 modes in the system, so we are effectively solving a coupled sytem of time-dependent ordinary differential equations of this order. Nevertheless, the linear parts of this system (the terms on the left-hand side of equations (3.3), (3.9)–(3.16)) can be solved implicitly using a Crank-Nicolson scheme, because the x and y dependence can be separated out. The nonlinear terms, however, are treated explicitly, because the large order of the system makes fully implicit methods very expensive. The numerical performance of this code has been discussed in Rotvig and Jones (2002). The spatial resolution provided by the Fourier-Chebyshev expansions has a rather abrupt threshhold which means that, if the truncation level is too small for the parameters of the run, the solution suffers explosive numerical instability however small the timestep, but once the resolution is high enough to maintain stability, the accuracy increases very rapidly as the number of modes is increased. In practice, this means that there is a fairly sharp optimum number of modes to use for any given set of parameter values. This optimum value increases as either the Ekman number is lowered or the Rayleigh number is increased. The principal practical difficulty is the very small timestep required for numerical stability. The exact reasons for this are not well-understood, though some light can be shed by considering the MAC wave dispersion relation (see below). The numerical method used for the time-stepping is a simple Euler predictor-corrector method, and the time-step is varied automatically as the integration proceeds so that the difference between the predictor and corrector solutions is maintained at a set level. This maintains accuracy and stability. If the solution is started with a small seed magnetic field, the timestep chosen by the code during the kinematic build-up phase is not far from that expected from the CFL condition, i.e., the timestep has to be small enough for the product of the maximum velocity (here the local magnetic Reynolds number) and the timestep to be less than the mesh size, which we can approximate as $1/\max(N_x, N_y, N_z)$. However, when the magnetic field starts to saturate, the timestep drops significantly: for the range of parameters considered below, the reduction can be a factor ten or more. As E is lowered, the timestep drops further (see Rotvig and Jones (2002) for details), and this effectively gives a barrier below which we cannot go in reducing E. Similar problems are experienced in spherical codes as E is lowered.

In view of this, it might seem a good idea to re-introduce inertia. However, the waves resulting from the balance between the inertial and Coriolis forces are the inertial waves, which have a natural timescale of days. The waves associated with buoyancy are internal gravity waves, though these usually manifest themselves in their unstable form as growing convective modes. The magnetic waves

are Alfvén waves, which typically have a timescale of a few years. (These are the analogue of the torsional oscillations that arise in the corresponding spherical system; because of the degeneracy of the plane layer, they have a greater significance here.) The magnetic fields grow in dynamo calculations on the eddy turnover timescale, which is the 10^5 year diffusion timescale d^2/η divided by $R_m \sim 300$. To establish that fields are not decaying through diffusion, it is necessary to run codes for a substantial fraction of a diffusion time, which in practice is at least 0.1 of the diffusion time, i.e., at least 10,000 years. It is clear that if waves on the timescale of days are going to appear in the simulation the timestep needs to be a small fraction of a day, which implies that a minimum of 10^8 timesteps will be needed per run. Even with high speed parallel processors, this is a severe restriction for a fully three-dimensional Navier-Stokes solver. We can overcome this difficulty either by slowing down the inertial waves and the Alfvén waves, by altering the rotation rate relative to the eddy turnover time (this is done in those codes that retain inertia by artificially taking $\nu = \kappa = \eta$), or by removing the inertial term entirely. The $\nu = \kappa = \eta$ approach has the disadvantage that waves, that in reality are on a different timescale from the dynamo modes, are now on the same timescale as the convective turnover in the simulation, and so may be strongly excited by the convection. This in turn can affect the generation mechanism, as evidenced by recent models of Busse (2002) in which inertial effects strongly influence the dynamo. For this reason we here exclude the inertial terms $D\mathbf{u}/Dt$ *ab initio*.

4. The hyperdiffusive and the LANS α-models

With the addition of isotropic hyperdiffusion to all three diffusing quantities, (3.3) and (3.9)–(3.16) become

$$\nabla_H^2[\partial_z f + E\nabla^2(1-\alpha_V^2\nabla^2)e] = \hat{\mathbf{z}}\cdot\boldsymbol{\nabla}\times(\mathbf{j}\times\mathbf{B}), \tag{4.1}$$

$$\nabla_H^2[\partial_z e - E\nabla^4(1-\alpha_V^2\nabla^2)f + qRa\theta] = \hat{\mathbf{z}}\cdot\boldsymbol{\nabla}\times\boldsymbol{\nabla}\times(\mathbf{j}\times\mathbf{B}), \tag{4.2}$$

$$\nabla_H^2[\partial_t - \nabla^2(1-\alpha_B^2\nabla^2)]g = -\hat{\mathbf{z}}\cdot\boldsymbol{\nabla}\times(\mathbf{u}\times\mathbf{B}), \tag{4.3}$$

$$\nabla_H^2[\partial_t - \nabla^2(1-\alpha_B^2\nabla^2)]h = -\hat{\mathbf{z}}\cdot\boldsymbol{\nabla}\times\boldsymbol{\nabla}\times(\mathbf{u}\times\mathbf{B}), \tag{4.4}$$

$$\partial_t\theta - q\nabla^2(1-\alpha_T^2\nabla^2)\theta + \nabla_H^2 f = -\mathbf{u}\cdot\boldsymbol{\nabla}\theta, \tag{4.5}$$

$$-U_y - E\partial_z^2(1-\alpha_V^2\partial_z^2)U_x = \hat{\mathbf{x}}\cdot\langle\mathbf{j}\times\mathbf{B}\rangle, \tag{4.6}$$

$$U_x - E\partial_z^2(1-\alpha_V^2\partial_z^2)U_y = \hat{\mathbf{y}}\cdot\langle\mathbf{j}\times\mathbf{B}\rangle, \tag{4.7}$$

$$[\partial_t - \partial_z^2(1-\alpha_B^2\partial_z^2)]b_x = \hat{\mathbf{x}}\cdot\langle\boldsymbol{\nabla}\times(\mathbf{u}\times\mathbf{B})\rangle, \tag{4.8}$$

$$[\partial_t - \partial_z^2(1-\alpha_B^2\partial_z^2)]b_y = \hat{\mathbf{y}}\cdot\langle\boldsymbol{\nabla}\times(\mathbf{u}\times\mathbf{B})\rangle. \tag{4.9}$$

Here α_V, α_B and α_T are the length scales associated with the three forms of hyperdiffusion. In principle, they can all be different, but in the numerical runs they are generally taken to have the same value. There is some numerical evidence to suggest that the temperature distribution is comparatively smooth for the parameter regime tested here (see e.g., figure 12 of Rotvig and Jones 2002) and so we have also done some runs with $\alpha_T = 0$. If the very small q regime could be accessed, we might expect high Péclet number solutions to emerge, in which case small length scales will reappear in the temperature field, so this issue should be left open.

The LANS α-model has recently been extended to the MHD case, and equations closely related to the hyperdiffusive equations have been proposed by Holm (2003) in what we shall call "Holm-MHD theory". Following the principles of Section 2, we introduce filtered (barred variables) and unfiltered (unbarred) variables with the relations

$$e = (1-\alpha^2\nabla^2)\bar{e}, \quad f = (1-\alpha^2\nabla^2)\bar{f},$$

$$g = (1-\alpha^2\nabla^2)\bar{g}, \quad h = (1-\alpha^2\nabla^2)\bar{h}, \quad \theta = (1-\alpha^2\nabla^2)\bar{\theta}, \tag{4.10}$$

$$U_x = (1-\alpha^2\partial_z^2)\bar{U}_x, \quad U_y = (1-\alpha^2\partial_z^2)\bar{U}_y,$$

$$b_x = (1-\alpha^2\partial_z^2)\bar{b}_x, \quad b_y = (1-\alpha^2\partial_z^2)\bar{b}_y. \tag{4.11}$$

The Holm-MHD equations then take the form

$$\nabla_H^2(\partial_z\bar{f} + E\nabla^2 e) = \hat{\mathbf{z}}\cdot\boldsymbol{\nabla}\times(\mathbf{j}\times\bar{\mathbf{B}}), \tag{4.12}$$

$$\nabla_H^2(\partial_z\bar{e} - E\nabla^4 f + qRa\bar{\theta}) = \hat{\mathbf{z}}\cdot\boldsymbol{\nabla}\times\boldsymbol{\nabla}\times(\mathbf{j}\times\bar{\mathbf{B}}), \tag{4.13}$$

$$\nabla_H^2(\partial_t\bar{g} - \nabla^2 g) = -\hat{\mathbf{z}}\cdot\boldsymbol{\nabla}\times(\bar{\mathbf{u}}\times\bar{\mathbf{B}}), \tag{4.14}$$

$$\nabla_H^2(\partial_t\bar{h} - \nabla^2 h) = -\hat{\mathbf{z}}\cdot\boldsymbol{\nabla}\times\boldsymbol{\nabla}\times(\bar{\mathbf{u}}\times\bar{\mathbf{B}}), \tag{4.15}$$

$$(\partial_t - q\nabla^2)\bar{\theta} + \nabla_H^2\bar{f} = -\bar{\mathbf{u}}\cdot\boldsymbol{\nabla}\bar{\theta}, \tag{4.16}$$

$$-\bar{U}_y - E\partial_z^2 U_x = \hat{\mathbf{x}}\cdot\langle\mathbf{j}\times\bar{\mathbf{B}}\rangle, \tag{4.17}$$

$$\bar{U}_x - E\partial_z^2 U_y = \hat{\mathbf{y}}\cdot\langle\mathbf{j}\times\bar{\mathbf{B}}\rangle, \tag{4.18}$$

$$\partial_t\bar{b}_x - \partial_z^2 b_x = \hat{\mathbf{x}}\cdot\langle\boldsymbol{\nabla}\times(\bar{\mathbf{u}}\times\bar{\mathbf{B}})\rangle, \tag{4.19}$$

$$\partial_t\bar{b}_y - \partial_z^2 b_y = \hat{\mathbf{y}}\cdot\langle\boldsymbol{\nabla}\times(\bar{\mathbf{u}}\times\bar{\mathbf{B}})\rangle. \tag{4.20}$$

Equations (4.12)–(4.20) are remarkably similar to the hyperdiffusive system (4.1)–(4.9), provided the hyperdiffusive variables are interpreted as the filtered variables of the Holm-MHD theory. The only difference is in the expression for the Lorentz force (in equations (4.12), (4.13), (4.17) and (4.18)), where the unfiltered current $\mathbf{j}$ and the filtered $\overline{\mathbf{B}}$ appear in the Holm equations, whereas in the hyperdiffusive system both a filtered current $\bar{\mathbf{j}}$ and a filtered $\bar{\mathbf{B}}$ are used (see also Subramanian, 2003).

5. Subgrid scale boundary conditions

The anisotropic hyperdiffusion models of Glatzmaier and Roberts and Kuang and Bloxham only enhanced the diffusion on spherical surfaces and not in the radial direction. This is convenient if a numerical method is used where the ϑ and ϕ dependence is represented by a spherical harmonic expansion. Thus they replaced the ∇^2 operator by a formula such as

$$(1 + \alpha\ell^3)\nabla^2 \tag{5.1}$$

where ℓ is the degree of the spherical harmonic of the expansion function. In some runs, the standard diffusion is used for harmonics of lower degree, hyperdiffusivity only being applied to the higher harmonics. Using a formula of the type (5.1) avoids the necessity of imposing extra boundary conditions at the inner core boundary and the core-mantle boundary. However, if we wish to avoid an unphysical anisotropy and instead adopt an isotropic hyperdiffusion, to avoid the criticisms of Grote *et al.* (2000), we must add boundary conditions in the radial direction. In our plane layer model this corresponds to additional boundary conditions at $z = \pm\frac{1}{2}$.

For the LANS α theory, it is helpful to think of the boundary conditions in terms of the variables $\mathbf{u}$ and $\overline{\mathbf{u}}$ related by (2.13). In the no-slip case, the most natural approach would be to set both $\mathbf{u}$ and $\overline{\mathbf{u}}$ to zero at the boundaries, but unfortunately this is not possible. We have three large scale boundary conditions, $\bar{f} = \bar{f}' = \bar{e} = 0$, to apply at each boundary, and we need two further subgrid scale conditions, because (4.10) and (4.11) involve second order operators. However, $e = f = f' = 0$ implies $\bar{f}'' = \bar{f}''' = \bar{e}'' = 0$ which is one too many conditions, so that the resulting problem is not well-posed. For the hyperdiffusive equations, it is more natural to force the barred variables to satisfy the large scale boundary conditions.

We next look at the energy equation, and attempt to choose the boundary conditions through the requirement that the surface integrals which appear should vanish. The energy equation from the Holm-MHD equations is formulated by taking the scalar product of the momentum equation with $\overline{\mathbf{u}}$. The viscous term then gives

$$\int \bar{\mathbf{u}}\cdot\boldsymbol{\nabla}^2\mathbf{u}\,d^3x = \oint_S [d\mathbf{s}\cdot\boldsymbol{\nabla}\mathbf{u}]\cdot\bar{\mathbf{u}} + \alpha_V^2\oint_S [d\mathbf{s}\cdot\boldsymbol{\nabla}\bar{\mathbf{u}}]\cdot\boldsymbol{\nabla}^2\bar{\mathbf{u}} - \int [(\boldsymbol{\nabla}\bar{\mathbf{u}})^2 + \alpha_V^2|\boldsymbol{\nabla}^2\bar{\mathbf{u}}|^2]\,d^3x. \tag{5.2}$$

The first surface term vanishes if the large scale boundary conditions $\bar{u}_i = 0$ are adopted. To rid ourselves of the second term we could impose $\partial_z\bar{u}_i = 0$. The z component of this is already zero ($\bar{u}_z = \nabla_H^2\bar{f}$, and $\bar{f}' = 0$), so the full set of boundary conditions is

$$\bar{f} = \bar{f}' = \bar{e} = \bar{e}' = \bar{f}'' = 0, \qquad \text{on} \qquad z = \pm\tfrac{1}{2}, \tag{5.3}$$

the first three being the large scale boundary conditions and the second two the subgrid scale boundary conditions. For the mean flow, we use

$$\bar{U}_x = \bar{U}_x' = \bar{U}_y = \bar{U}_y' = 0 \qquad \text{on} \qquad z = \pm\tfrac{1}{2}. \tag{5.4}$$

We have adopted (5.3) and (5.4) in most of the numerical simulations (see Section 7 below). We found that they are numerically satisfactory, in that no new numerical instabilities are introduced by this choice of subgrid scale boundary conditions, and in Section 6 below we find that they do not lead to substantial changes at the onset of convection. This choice is not the only possible one though, because $\partial_{kk}\bar{u}_H$ vanishes if $\bar{e}'' = \bar{f}'''' = 0$, and this also gives a well-posed system. An alternative set of mechanical boundary conditions is discussed in Appendix B, which also makes the viscous dissipation positive definite whatever the flow in the layer, a desirable property for a hyperdiffusive system.

We now turn to the magnetic boundary conditions. There is here no problem with applying (3.19) and (3.20) to both the filtered and unfiltered fields. In terms of the filtered variables we then have (for the Fourier component (l, m))

$$\bar{g} = \bar{g}'' = 0, \quad \bar{h}'_{lm} = \mp a\bar{h}_{lm}, \quad \bar{h}'''_{lm} = \mp a\bar{h}''_{lm} \qquad \text{on} \qquad z = \pm\tfrac{1}{2}. \tag{5.5}$$

The mean field components can be treated similarly to give

$$\bar{b}_x = \bar{b}_y = \bar{b}''_x = \bar{b}''_y = 0 \qquad \text{on} \qquad z = \pm\tfrac{1}{2}. \tag{5.6}$$

These are the magnetic boundary conditions we have used for the numerical simulations in Section 7.

The magnetic energy integrals have integrated surface terms but, unlike the kinetic energy integrals, they do not vanish because the magnetic field is non-zero outside the layer, so that magnetic energy flows through the boundaries. For the hyperdiffusive system (4.1)-(4.9) we would like to ensure that the ohmic dissipation is positive:

$$\int \bar{\mathbf{j}}\cdot(1-\alpha_B^2\nabla^2)\bar{\mathbf{j}}\,dv = \int \bar{\mathbf{j}}\cdot\bar{\mathbf{j}}\,dv - \alpha_B^2\oint_S \bar{\mathbf{j}}\cdot\partial_z\bar{\mathbf{j}}\,dS + \alpha_B^2\int(\partial_z\bar{\mathbf{j}})^2\,dv > 0. \tag{5.7}$$

The surface integral contains parts involving $\bar{b}_x$, $\bar{b}_y$, $\bar{g}$ and $\bar{h}$, but the parts involving $\bar{b}_x$, $\bar{b}_y$, and $\bar{g}$ vanish if (5.5) and (5.6) are employed, while the part involving $\bar{h}$ is negative if (5.5) is used. We conclude that (5.5) and (5.6) are suitable boundary conditions for the hyperdiffusive system, but note that, as for the case of the velocity boundary conditions, the choice made through requiring the surface terms to have appropriate properties does not lead to a unique set of boundary conditions. An alternative is discussed in Appendix A.

Our choice of boundary conditions seems physically reasonable and is apparently numerically stable, but a clearer physical motivation for them is desirable. In the case of the Holm-MHD equations this would require an analysis of the expected form of the turbulent fluctuations near the boundaries. See Appendix B for a further discussion.

In cases where a thermal hyperdiffusion is used an additional boundary condition on the temperature is required. This was taken to be $\bar{\theta}' = 0$, so the full thermal boundary conditions used were

$$\bar{\theta} = \bar{\theta}' = 0 \qquad \text{on} \qquad z = \pm\tfrac{1}{2}. \tag{5.8}$$

Additional boundary conditions on θ are not required for the Holm-MHD equations.

6. Linear theory

Although the dynamo problem is fully nonlinear, there are two related linear problems that can give some insight into the behaviour of the nonlinear system. The nonlinear system is fully three-dimensional, so that it is not practical to carry out detailed explorations of parameter space, but insights from linear theory are crucial for interpreting the output from the limited number of fully nonlinear runs it is possible to perform.

The first linear problem is to examine the effect of hyperdiffusion on the nonmagnetic onset of rotating convection. General features such as the boundary layer structure may persist into the nonlinear regime. The second linear problem is the magnetoconvection problem with a uniform imposed magnetic field, which gives rise to the MAC wave dispersion relation.

The linearised equations for the onset of convection are

$$2\hat{\mathbf{z}}\times\mathbf{u} = -\boldsymbol{\nabla}p + E\nabla^2(1-\alpha_V^2\nabla^2)\mathbf{u} - Ra\theta\hat{\mathbf{z}}, \tag{6.1}$$

$$\partial_t\theta = u_z + \nabla^2(1-\alpha_T^2\nabla^2)\theta. \tag{6.2}$$

Here we have used d^2/κ as the unit of time. These are supplemented by the no-slip boundary conditions (3.18) and the constant temperature boundary condition (3.21). The main results from the standard linear theory are given in Fearn *et al.* (1988) and here we just summarise the differences introduced by the hyperdiffusive terms, which we assume are small. We can best understand the behaviour if we take the limit $E \to 0$. In the classical problem, the horizontal wavenumber at marginal stability is then $\mathrm{O}(E^{1/3})$ and there is an Ekman layer of thickness $\mathrm{O}(E^{1/2})$. The dissipation term $E\nabla^2\mathbf{u}$ in the interior is $O(E^{1/3})\mathbf{u}$, while the dissipation in the Ekman layer is slightly smaller at $\mathrm{O}(E^{1/2})\mathbf{u}$ so the interior dissipation dominates. Stress-free boundaries allow a solution with $\theta = \theta_0 \cos \pi z$, which gives marginal stability at

$$Ra = \frac{\pi^2[1+\alpha_T^2(\pi^2+k^2)]}{E(\pi^2+k^2)[1+\alpha_V^2(\pi^2+k^2)]} + \frac{E(\pi^2+k^2)^3[1+\alpha_V^2(\pi^2+k^2)][1+\alpha_T^2(\pi^2+k^2)]}{k^2} \tag{6.3}$$

The critical horizontal wavenumber k greatly exceeds π and is therefore determined by

$$\frac{k^6(1+\alpha_V^2k^2)^2[2+3k^2(\alpha_V^2+\alpha_T^2)+4k^4\alpha_V^2\alpha_T^2]}{1+2k^2\alpha_V^2+k^4\alpha_V^2\alpha_T^2} = \frac{E^2}{\pi^2}. \tag{6.4}$$

It is now clear that if

$$\alpha_V \ll \left(\frac{E^2}{2\pi^2}\right)^{\frac{1}{6}} \quad \text{and} \quad \alpha_T \ll \left(\frac{E^2}{2\pi^2}\right)^{\frac{1}{6}} \tag{6.5}$$

the hyperdiffusive terms make only a small change to the critical wavenumber for convection. The situation is not greatly changed if no-slip boundaries are used. One may reasonably hope that, provided criteria (6.5) are satisfied, the behaviour of the convection in the interior will not be dramatically altered by the addition of hyperdiffusion. Of course, the smaller length scales generated by nonlinear interactions, which can include for example sharp plume boundaries or regions of rapidly varying magnetic field, will be affected. The hope is that this modification will represent to some extent the turbulent processes at work in the fluid.

We also need to examine the effect of hyperdiffusion on the boundary layers. To do this, we return to (6.3), but now replace π^2 by $-k_z^2$, where $1/k_z$ is the boundary layer thickness, which is much smaller (at low E) than $1/k$. The equation for k_z becomes

$$E^2k_z^4(1-\alpha_V^2k_z^2)^2 = -1. \tag{6.6}$$

The classical limit is

$$\alpha_V \ll E^{1/2}, \tag{6.7}$$

and then the smallest roots for k_z (which produce the thickest boundary layer) are the classical Ekman layer values $k_z = (\pm 1 \pm i)/\sqrt{2E}$. The solutions corresponding to two of these roots are rejected from the boundary layer solution because they grow as we move into the interior, and the remaining two are determined by the boundary conditions and the matching to the interior flow. Since (6.6) is of eighth order there are four more solutions, of which two can be rejected as they do not decay as we move into the interior. The remaining two are determined by the additional subgrid scale boundary conditions. This leads to an interior boundary layer of thickness α_V lying within the Ekman boundary layer itself of thickness $O(E^{1/2})$. This could cause numerical resolution problems; the need to resolve the Ekman boundary layer is already a serious constraint on the numerical code, and we do not wish to exacerbate this. If there were no magnetic field, we could choose our subgrid scale boundary conditions to eliminate this interior layer. However, in the presence of a magnetic field having the expected O(1) Elsasser number, the Ekman layer becomes an Ekman-Hartmann layer whose thickness varies depending on the local field strength near the boundary as the computation progresses. It is not a practical proposition to choose boundary conditions that always eliminate the α_V boundary layer in a dynamo code.

In practice we therefore choose α_V so that it is of order $E^{1/2}$. The structure of the Ekman boundary layer is affected, but its thickness remains of $\mathrm{O}(E^{1/2})$. The eight roots of (6.6) are then

$$k_z = \pm\left[\frac{1 \pm \sqrt{1 \pm 4i\alpha_V^2E^{-1}}}{2\alpha_V^2}\right]^{1/2} \tag{6.8}$$

four of which decay as we move into the interior and hence are the basis of the boundary layer solution. This change in the boundary layer structure may be a cause for concern, but we should remember that an $O(E^{1/2})$ boundary layer does not affect the onset of convection at leading order, so we do not expect the interior convection to be strongly affected. The most significant change from the alteration of the Ekman boundary layer is probably to the geostrophic flows induced by the magnetic field. Boundary layer friction can play a role in the dynamics of these motions, and it is probable that this is connected with the stabilization that hyperdiffusion produces.

To see the effect of the hyperdiffusion on the marginal stability problem for the typical values of hyperdiffusion used, we have constructed Table 1 using a linear stability code with no-slip boundaries, and the subgrid scale boundary conditions in (5.3).

E	α_V^2	α_T^2	minimizing k	Ra
0.001	0	0	10.820	71.085
0.001	0.0001	0.0001	10.710	72.725
0.001	0.0002	0.0002	10.590	73.417
0.001	0.0005	0.0005	10.277	75.087
0.001	0.001	0.001	9.861	77.514
0.0005	0	0	13.870	88.224
0.0005	0.0001	0.0001	13.607	89.876
0.0005	0.0002	0.0002	13.367	90.663
0.0005	0.0002	0.0005	13.075	95.924
0.0005	0.0005	0.0002	13.056	87.948
0.0005	0.0005	0.0005	12.785	92.851
0.0005	0.001	0.001	12.070	96.246
0.0002	0	0	19.248	119.888
0.0002	0.0001	0.0001	18.542	121.520
0.0002	0.0002	0.0002	17.997	122.789
0.0002	0.0005	0.0005	16.797	126.809
0.0002	0.001	0.001	15.455	133.005

Table 1. The minimum Rayleigh number Ra and the corresponding horizontal wavenumber k are tabulated as a function of Ekman number E and the hyperdiffusivities α_V^2 and α_T^2.

The other relevant linear problem is the magnetoconvection problem, that is convection in the presence of an imposed magnetic field $\mathbf{B_0}$. We return to the magnetic diffusion time-scale, so the system studied is

$$\partial_z \mathbf{u} = (\mathbf{B_0}\cdot\boldsymbol{\nabla})\mathbf{j} + E\nabla^2(1-\alpha_V^2\nabla^2)\boldsymbol{\zeta} + \boldsymbol{\nabla}\times(qRa\theta\hat{\mathbf{z}}), \tag{6.9}$$

$$\partial_t \mathbf{b} = (\mathbf{B_0}\cdot\boldsymbol{\nabla})\mathbf{u} + \nabla^2(1-\alpha_B^2\nabla^2)\mathbf{b}, \tag{6.10}$$

$$\partial_t \theta = u_z + q\nabla^2(1-\alpha_T^2\nabla^2)\theta, \tag{6.11}$$

where $\boldsymbol{\zeta} = \boldsymbol{\nabla}\times\mathbf{u}$. We seek disturbances of the form $\exp i(\mathbf{k}\cdot\mathbf{x} - \omega t)$, and write

$$k_V^2 = k^2(1+\alpha_V^2 k^2), \quad k_B^2 = k^2(1+\alpha_B^2 k^2), \quad k_T^2 = k^2(1+\alpha_T^2 k^2). \tag{6.12}$$

The dispersion relation is

$$\Big(\frac{(\mathbf{B_0}\cdot\mathbf{k})^2}{k_B^2 - i\omega} + Ek_V^2\Big)\Big(\frac{(\mathbf{B_0}\cdot\mathbf{k})^2}{k_B^2 - i\omega} + Ek_V^2 - \frac{qRak_\perp^2}{k^2(qk_T^2 - i\omega)}\Big) + \frac{k_z^2}{k^2} = 0, \tag{6.13}$$

where k_z is the z-component of the wavevector, and $k_\perp$ is the magnitude of the horizontal component. In the absence of all diffusion this reduces to the MAC wave dispersion relation (Braginsky, 1964)

$$\omega^2 = \frac{k^2(\mathbf{B_0}\cdot\mathbf{k})^2}{k_z^2}\Big((\mathbf{B_0}\cdot\mathbf{k})^2 - \frac{qRak_\perp^2}{k^2}\Big) \tag{6.14}$$

which describes slow waves in the Earth's core. When the Elsasser number $\Lambda = B_0^2/2\Omega\mu\rho\eta$ is order one, the timescale of these waves is the magnetic diffusion time for the core. For those modes where the Rayleigh number is large enough to make negative the term between large brackets in (6.14), the waves become growing convective modes. Although the timescale for these modes is generally on the dynamo timescale, modes with k_z small or zero have much higher frequencies, and this causes numerical difficulties (Walker *et al.*, 1998). These are the geostrophic modes where there is no longer a balance between Coriolis force and Lorentz force. Either Taylor's constraint is satisfied, which in our plane layer means the z-averaged Lorentz force over every vertical line must vanish, or any residual z-averaged component has to be balanced by viscous forces. This can lead to large accelerations in the velocity field. If we set $k_z = 0$ in (6.13), the toroidal and poloidal components separate, and we obtain

$$\omega = -i\Big(k_B^2 + \frac{(\mathbf{B_0}\cdot\mathbf{k})^2}{Ek_V^2}\Big), \quad \omega = -i\Big(k_B^2 + \frac{k^2(\mathbf{B_0}\cdot\mathbf{k})^2 - qRak_\perp^2}{k^2Ek_V^2}\Big). \tag{6.15}$$

The first of these describes damped modes, and the second either damped or growing convective modes. The fastest growing modes are those with "plate-like" motions in which $\mathbf{k}$ is perpendicular to both the rotation axis and the field, corresponding to motions in the plane containing the rotation and magnetic field vectors (Braginsky and Meytlis, 1990). In a nonlinear system, the growth of these modes will be controlled by nonlinearity, but the appearance of E in the denominator indicates that numerical difficulties are likely at small E. The fact that the first solution in (6.15) (which belongs to the toroidal e component of the velocity) is strongly damped might give rise to the naïve hope that these modes would not matter in a numerical simulation. In reality, strongly damped modes make the system stiff, and the timestep may be expected to drop to a value for which this fast decay on a timescale E/Λ has to be resolved.

7. Numerical simulations

To test how isotropic hyperdiffusion and the Holm-MHD model behave in numerical simulations, we have performed a series of runs with our plane layer convective dynamo model. Numerical details of the implementation can be found in Jones and Roberts (2000) and Rotvig and Jones (2002). The aim here is simply to test the codes: the implications for dynamo theory are discussed in the previous papers. We have concentrated on three sets of parameter values. Benchmark (i) is an "easy" parameter set with $E = 10^{-3}$, $q = 1$, $Ra = 1000$ and a box size such that the $\ell = m = 1$ horizontal wavenumber is $k_x = k_y = 2\pi\sqrt{2}$ (Run G of Jones and Roberts (2000)). This Rayleigh number is about 14 times the minimum plane layer value (see Table 1), and the restriction on the choice of horizontal wavelengths imposed by the box size only increases the critical value slightly. A cubical periodic box has wavenumber 2π; the reason for choosing a slightly smaller box is that at these wavenumbers the dynamo is not subcritical, i.e., the magnetic field grows from a small random seed field. A resolution of only 16^3, i.e., a truncation level of $N_x = N_y = N_z = 16$, is just adequate for this case, but all runs were performed at 32^3 resolution. The second benchmark (ii) is $E = 5\times10^{-4}$, $q = 1$ and $Ra = 2500$, with $\alpha = \beta = 2\pi$. This is also a self-excited dynamo, but the higher Ra and lower E make this a somewhat more demanding benchmark. This was run mainly at 32^3, though it was also thoroughly tested at $N_x = N_y = N_z = 32\times32\times48$, as the z-resolution is slightly more critical than the x, y resolution for this run. It was also checked against a longer multiprocessor run at $48\times48\times64$. Our final bechmark (iii) is $E = 2\times10^{-4}$, $Ra = 5000$, $q = 0.5$, again with the cubical box $\alpha = \beta = 2\pi$. The higher Ra and lower q in particular makes benchmark (iii) considerably more demanding. It has not yet been investigated as thoroughly as the others; in the absence of hyperdiffusion a truncation of $32\times32\times64$ is an adequate resolution to avoid explosive numerical instability.

All three benchmarks are kinematic dynamos, in the sense that, when started from a small random seed, the magnetic field grows and then saturates. As in previous work, it is notable that because the convective flow is highly time-dependent, particularly for the higher Rayleigh number benchmarks, field growth is an erratic process, comparatively short bursts of generation being followed by longer periods of consolidation. This means that the onset of dynamo action is much more easiy studied than the saturated regime. For example, the timestep for the saturated range of benchmark (ii) is typically twenty times less than for the kinematic phase.

Benchmark	Hyperdiffusion	Typical timestep
(i)	None	8×10^{-6}
(ii)	None	5×10^{-7}
(iii)	None	2×10^{-7}
(i)	Holm-MHD $\alpha^2 = 0.0002$	10^{-5}
(ii)	Holm-MHD $\alpha^2 = 0.0002$	6×10^{-7}
(ii)	All 3, $\alpha^2 = 0.0005$	4×10^{-6}
(iii)	All 3, $\alpha^2 = 0.0005$	2×10^{-6}
(iii)	All 3, $\alpha^2 = 0.0010$	4×10^{-6}
(ii)	**u**, **B** only, $\alpha^2 = 0.0005$	4×10^{-6}

Table 2. The typical timestep taken in the saturated regime for various runs.

As outlined above, a major constraint is the small timestep necessary in dynamo codes, so in Table 2 we give the typical timestep in the saturated regime needed to maintain numerical stability. The timestepping procedure used is a simple predictor-corrector scheme. At each step, the maximum relative change of the variables is monitored, and if it is more than 10^{-3} in any Chebyshev-Fourier component, the timestep is halved until the relative change is below the threshhold. If the relative change is less than 2×10^{-5} the timestep is doubled. In this way, the code chooses its own timestep. Any attempt to enforce a larger step than that selected by the code rapidly results in numerical instability. We here remark that the linear terms are dealt with implicitly, and the nonlinear terms (the Lorentz force, the nonlinear induction and the temperature advection) are treated explicitly, as usual in pseudo-spectral codes.

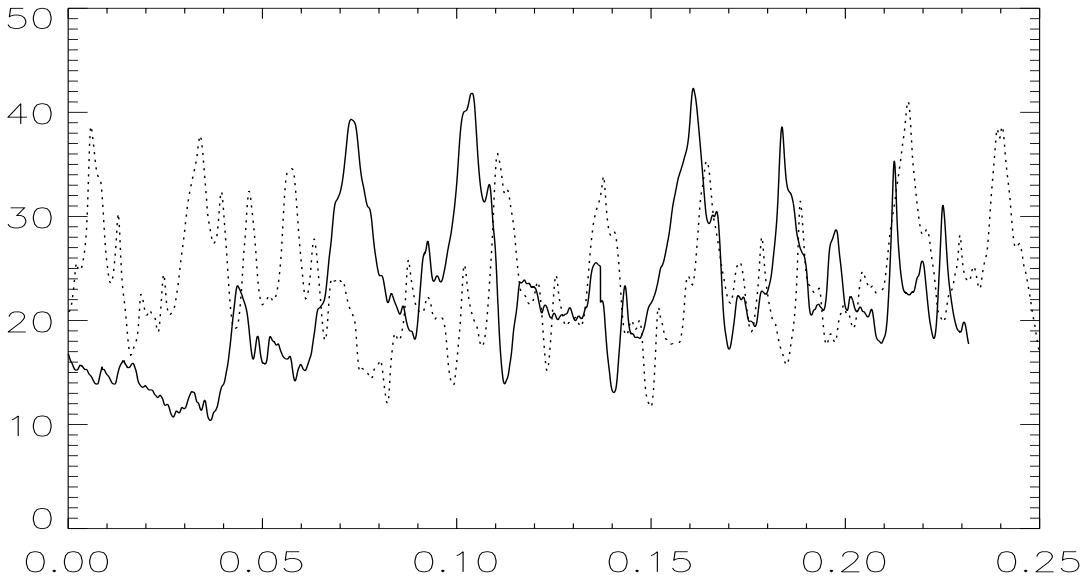

Figure 1. Benchmark (ii), $Ra = 2500$, $q = 1$, $E = 0.0005$. Solid line, plot of magnetic energy against time with no hyperdiffusion, average 22.24. Dotted line, plot of magnetic energy against time with hyperdiffusion $\alpha_V^2 = \alpha_B^2 = \alpha_T^2 = 0.0005$, *i.e.* equal hyperdiffusion applied to all three diffusing quantities. Average 23.86.

In Figure 1 we compare the time-dependence of the magnetic energy for benchmark (ii) both without hyperdiffusivity and with hyperdiffusivity. In this case all three hyperdiffusions were used, and all set equal to $\alpha^2 = 0.0005$. The equations used here are (4.1)–(4.9), with boundary conditions (5.3)–(5.6). The equivalent plots for the kinetic energy are shown in Figure 2. Note that, even if the comparison runs are started from the same data file, they will soon begin to diverge because there is chaotic time-dependence with sensitivity to initial conditions. We can therefore only compare

statistical quantities such as the mean magnetic field energy. It is clear from Figures 1 and 2 that the hyperdiffusion is not affecting either the kinetic energy or the magnetic energy very greatly, and indeed it would require a very long run to establish any significant difference between the plots. Note also that it is not only the average energy that is similar, but also the amplitude of the peaks and troughs and the frequency of their occurrence.

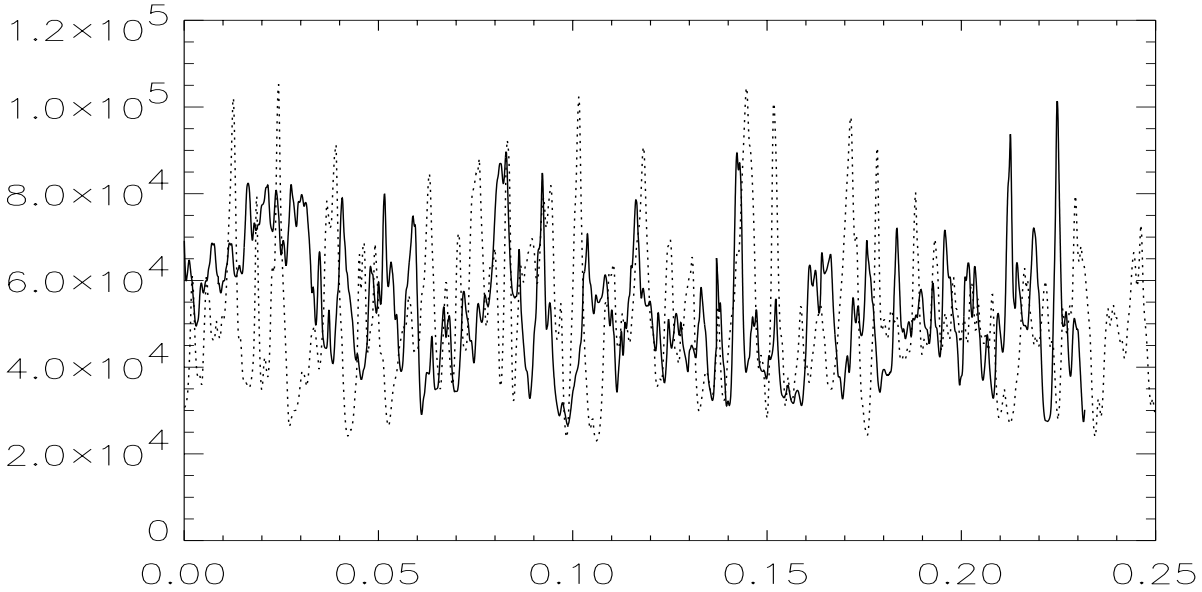

Figure 2. Benchmark (ii), $Ra = 2500$, $q = 1$, $E = 0.0005$. Solid line, plot of kinetic energy against time with no hyperdiffusion, average 53,141. Dotted line, plot of kinetic energy against time with hyperdiffusion $\alpha_V^2 = \alpha_B^2 = \alpha_T^2 = 0.0005$, *i.e.* equal hyperdiffusion applied to all three diffusing quantities. Average 51,604.

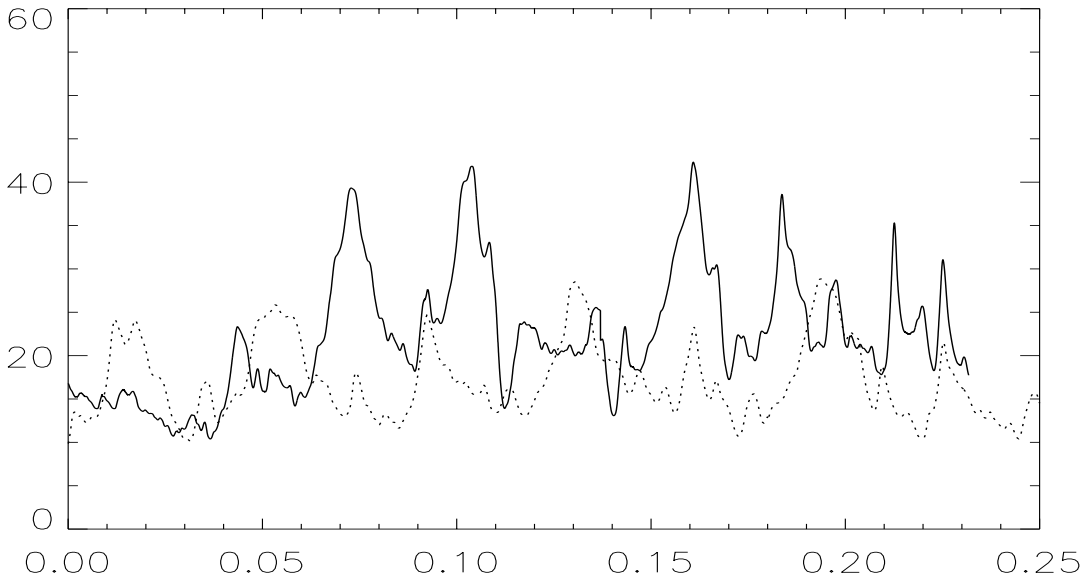

Figure 3. Benchmark (ii), $Ra = 2500$, $q = 1$, $E = 0.0005$. Solid line, plot of magnetic energy against time with no hyperdiffusion, average 22.24. Dotted line, plot of magnetic energy against time with hyperdiffusion $\alpha_V^2 = \alpha_B^2 = 0.0005$, $\alpha_T^2 = 0$, so hyperdiffusion applied to the momentum and induction equations but not the temperature equation. Average 17.46.

In Figures 3 and 4 we present the same plots, but for the case where there is magnetic and viscous hyperdiffusion, but no thermal hyperdiffusion. The timestep and general stability of the code has similar characterics to the case where all three hyperdiffusions are present, but now there is a significant difference between the hyperdiffusive and non-hyperdiffusive solutions.

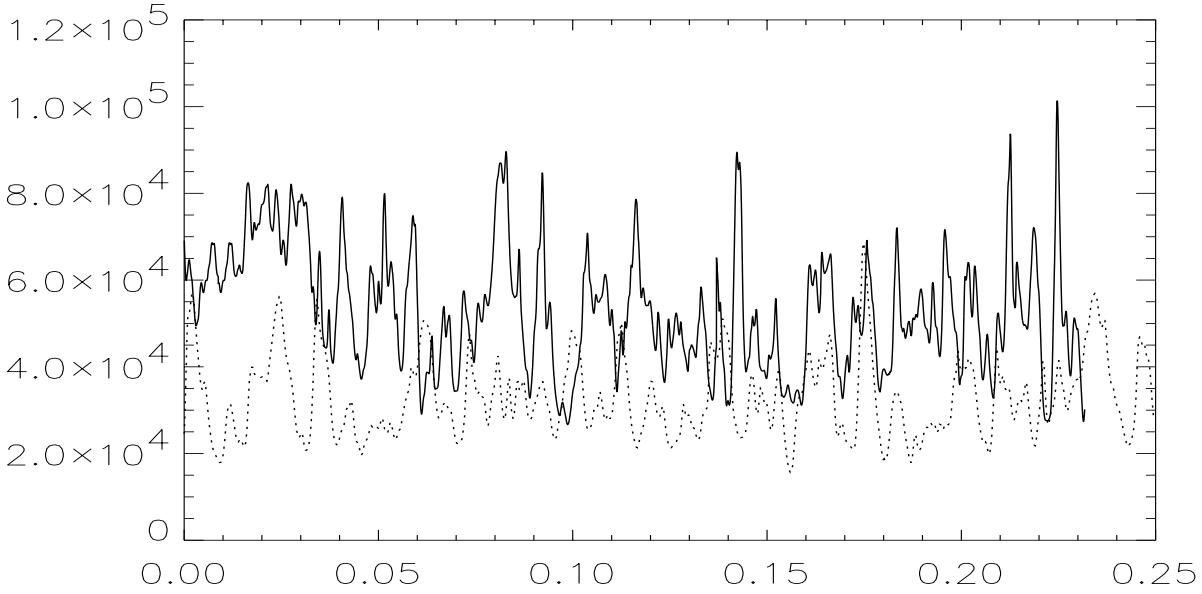

Figure 4. Benchmark (ii), $Ra = 2500$, $q = 1$, $E = 0.0005$. Solid line, plot of kinetic energy against time with no hyperdiffusion, average 53,141. Dotted line, plot of kinetic energy against time with hyperdiffusion $\alpha_V^2 = \alpha_B^2 = 0.0005$, $\alpha_T^2 = 0$, so hyperdiffusion applied to the momentum and induction equations but not the temperature equation. Average 32,266.

The hyperdiffusive solutions have significantly smaller average magnetic and kinetic energies than the non-hyperdiffusive solutions and this persists if the run is extended. This result seems surprising at first, because one might expect that removing a hyperdiffusion and replacing it by regular diffusion would increase the energies, not decrease them. However, by removing the temperature hyperdiffusion while retaining the magnetic field hyperdiffusion we have in effect decreased q. It is well-known that lowering q makes dynamo action considerably more difficult, so it is less surprising that the magnetic energy is reduced by the removal of the thermal hyperdiffusion. The fall in the kinetic energy is more unexpected, because the linear results in Table 1 suggest that increasing the thermal hyperdiffusion raises the critical Rayleigh number, and so we would expect removing thermal hyperdiffusion would increase the kinetic energy. To investigate this effect we switched off the Lorentz force, and noted that the kinetic energy was still larger with thermal hyperdiffusion than without it, so this is not primarily a magnetic effect. Contour plots of the temperature and velocity suggest that it is the effect of hyperdiffusion on the thermal boundary layer that is responsible. With thermal hyperdiffusion in force, the thermal boundary layers close to $z = \pm\frac{1}{2}$ are thicker, and this allows convection to be more vigorous; recall that in benchmark (ii) the Rayleigh number is well above critical. This highlights a difficulty with using hyperdiffusion when boundary layers play an important role in the solution.

In Figures 5 and 6 we give the magnetic and kinetic energy plots for benchmark (i) and the Holm-MHD equations. From Table 2, we see that the stability of the system is reduced by introducing the unbarred $\mathbf{j}$ into the Lorentz force, so that a comparison with benchmark (ii) would be time consuming, though preliminary runs suggest that the main features are similar for both benchmark cases. The modification of the Lorentz force term does not appear to have a great effect, and the general behaviour of the non-hyperdiffusive system is maintained. The Holm-MHD equations have only hyperdiffusion in magnetic field and momentum, so we might expect the magnetic and kinetic energies to be reduced, as in the comparison between Figures 1 and 2 and Figures 3 and 4. Figures 5 and 6 show that this is indeed the case, and this effect seems to be stronger than any effect due to the modification of the Lorentz force term. We have also run this case with the boundary conditions given in Appendix A (A5-A10), and Appendix B (B9-B10). These also gave stable numerical integrations, and the change in boundary conditions did not significantly affect the timestep.

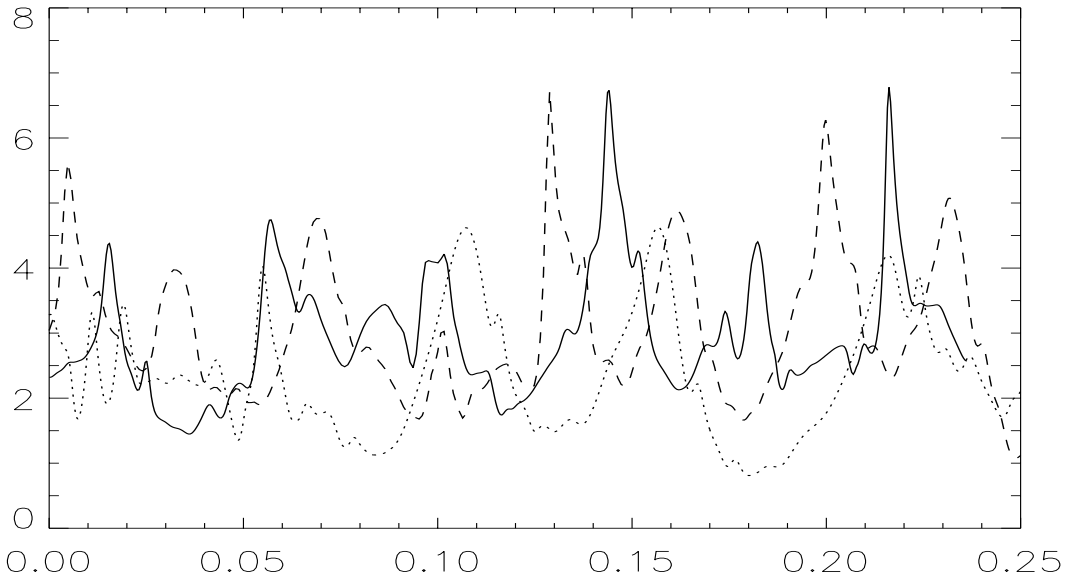

Figure 5. Benchmark (i), $Ra = 1000$, $q = 1$, $E = 0.0010$, $k_x = k_y = 2\sqrt{2}$. Solid line, plot of magnetic energy against time with no hyperdiffusion, average 2.9692. Dotted line, plot of magnetic energy against time using the Holm model with $\alpha^2 = 0.0002$ and boundary conditions (5.3-5.6), average 2.4200. Dashed line, plot of magnetic energy against time using the Holm model with $\alpha^2 = 0.0002$ and boundary conditions in Appendices A and B. Average 2.9193.

Changing the magnetic boundary conditions from (5.5-5.6) to (A5-A10) appears not to make a great difference, but the Appendix B mechanical conditions affect the boundary layers and this increases the kinetic energy significantly and the magnetic energy somewhat. Interestingly, this compensates the drops in these quantities found when using (5.3-5.4), so that the Appendix B boundary conditions give the best fit to the non-hyperdiffusive results when the Holm-MHD equations are used.

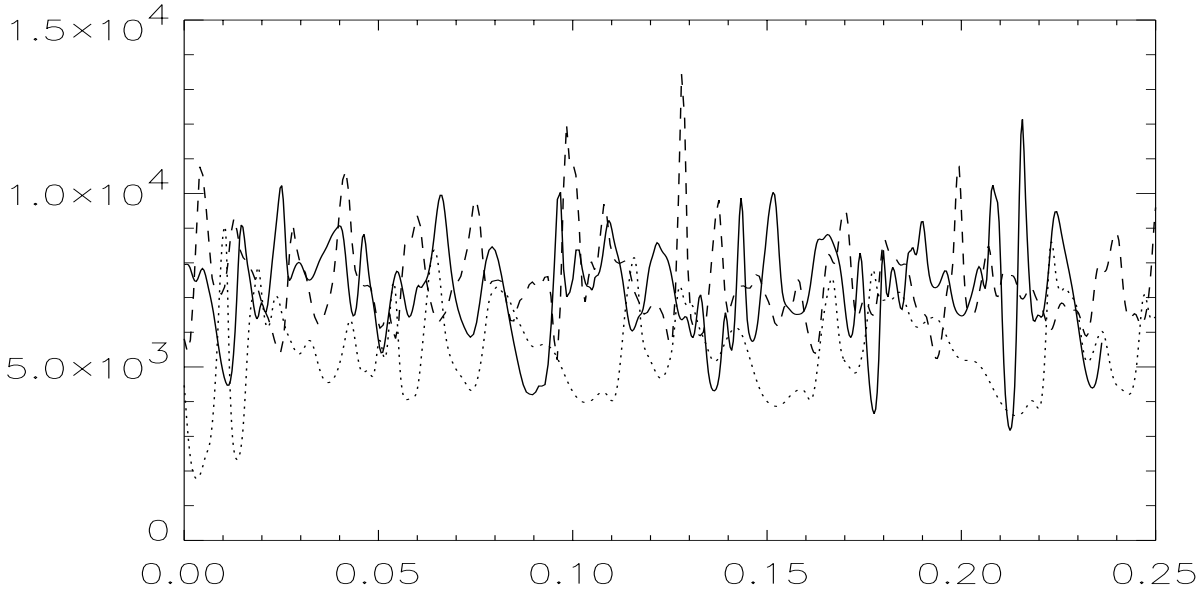

Figure 6. Benchmark (i), $Ra = 1000$, $q = 1$, $E = 0.0010$, $k_x = k_y = 2\sqrt{2}$. Solid line, plot of kinetic energy against time with no hyperdiffusion, average 7205.6. Dotted line, plot of kinetic energy against time using the Holm model with $\alpha^2 = 0.0002$ and boundary conditions (5.3-5.6), average 5410.6. Dashed line, plot of kinetic energy against time using the Holm model with $\alpha^2 = 0.0002$ and boundary conditions in Appendices A and B. Average 7506.5.

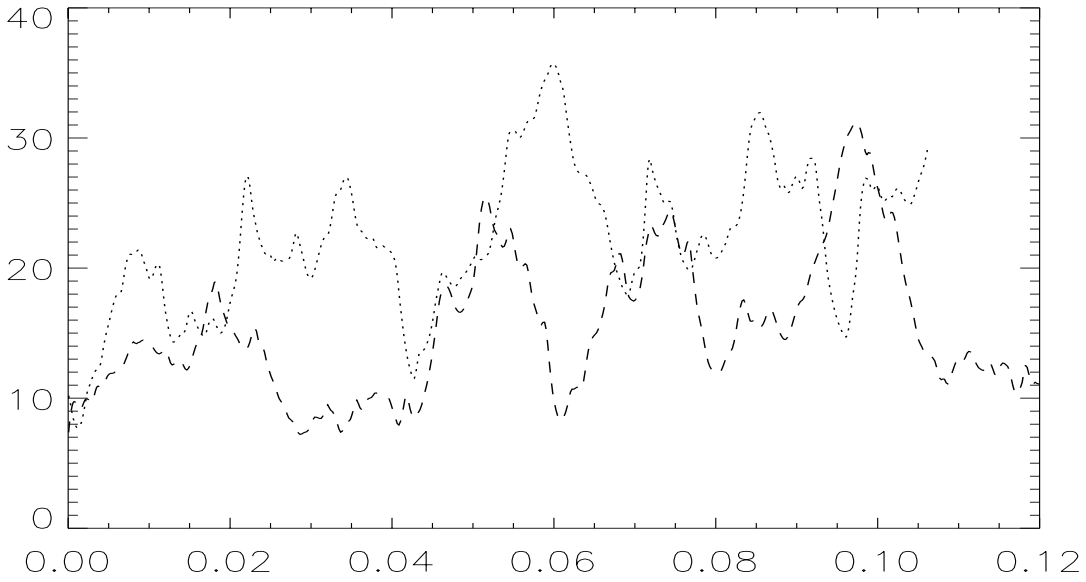

Figure 7. Benchmark (iii), $Ra = 5000$, $q = 0.5$, $E = 0.0002$. Dotted line, plot of magnetic energy against time with hyperdiffusion $\alpha_V^2 = \alpha_B^2 = 0.0005$, $\alpha_T^2 = 0.0005$, average 22.11. Dashed line: plot of magnetic energy against time with hyperdiffusion $\alpha_V^2 = \alpha_B^2 = \alpha_T^2 = 0.001$, average 17.59.

Finally in Figures 7 and 8 we have examined the behaviour of hyperdiffusive runs (with all three hyperdiffusivities) for benchmark (iii), the most demanding case. We plan to do integrations of this case with no hyperdiffusion, but this will require a great many processor hours to establish the behaviour definitively. By comparison, the hyperdiffusive runs can be performed quite quickly. By comparing the two cases α^2 =0.0005 and α^2 =0.001, we can extrapolate to the case of zero hyperdiffusion, and it will be an interesting test of the usefulness (or otherwise) of hyperdiffusivity to see if this predicted behaviour does in fact occur when the non-hyperdiffusive equations are integrated.

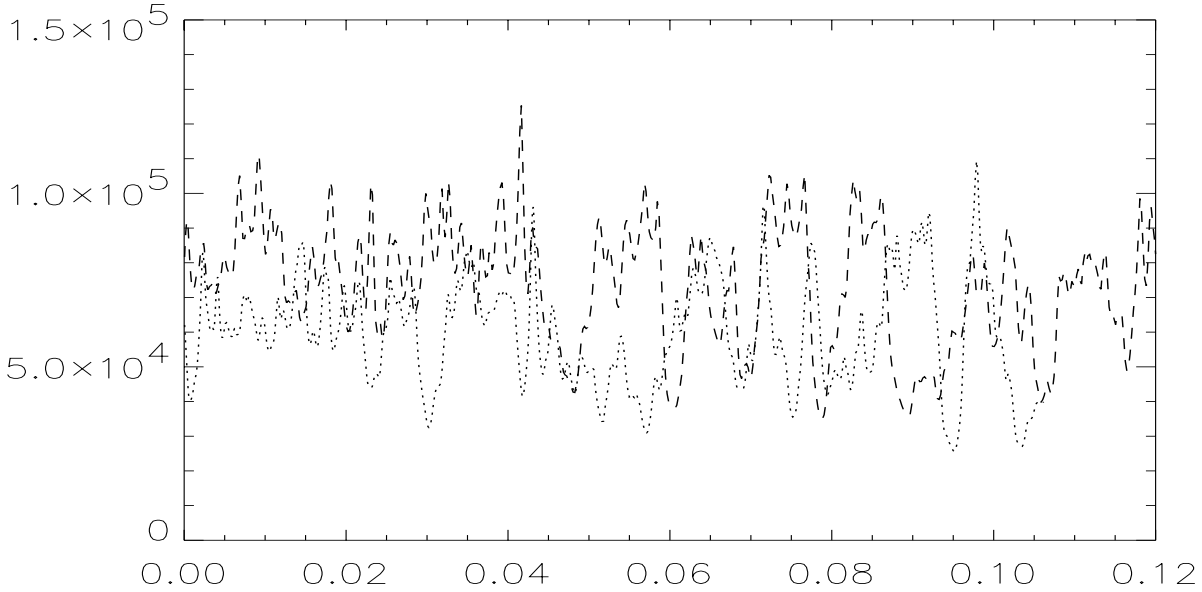

Figure 8. Benchmark (iii), $Ra = 5000$, $q = 0.5$, $E = 0.0002$. Dotted line, plot of kinetic energy against time with hyperdiffusion $\alpha_V^2 = \alpha_B^2 = 0.0005$, $\alpha_T^2 = 0.0005$, average 59,672. Dashed line: plot of kinetic energy against time with hyperdiffusion $\alpha_V^2 = \alpha_B^2 = \alpha_T^2 = 0.001$, average 69,952.

Another encouraging feature of the cases where all three hyperdiffusions are used is that the ratio of poloidal to toroidal components is not greatly affected. An important observation from the anisotropic hyperdiffusive simulations of Grote *et al.* (2000) was that hyperdiffusion strongly suppressed the poloidal components of the magnetic field in comparison with the toroidal components, thus changing the whole nature of the large scale magnetic field. We find no corresponding effect in these plane layer simulations.

8. Conclusions

Convection-driven dynamo models have great potential in helping us to understand the dynamics of planetary interiors, and this impacts on many areas of scientific activity. There is therefore a strong motivation for developing numerical schemes that will allow us to integrate the equations without requiring overwhelming computer resources. The use of hyperdiffusion, even when small coefficients are put in front of the hyperdiffusive terms, gives a remarkable amount of numerical stabilisation, so it is a very tempting way forward. It is also true that all numerical geodynamo simulations use some form of turbulent dissipation, and it is by no means obvious that merely increasing the numerical value of the regular diffusion terms is the best physical representation of these terms.

Generally, the isotropic hyperdiffusion appears to give quite similar behaviour to the non-hyperdiffusive benchmarks, though more work needs to be done before this can be asserted positively. Interestingly, the best results appear to be given when all the diffusive operators are treated in the same way. It appears that upsetting the ratios between the various diffusive processes has more effect than adding in hyperdiffusion to all diffusing quantities. This study has also shed some more light on the nature of the numerical instabilities that make the dynamo problem so hard to solve. Of particular note is the fact that when the magnetic field is strong, the timestep decreases by a factor of at least ten in the absence of hyperdiffusion. It is possible that this is due in part to the geostrophic modes having a rather singular behaviour, in which case there may be alternative ways of stabilising the system other than by invoking hyperdiffusion.

The issue of the boundary conditions to be used is not yet fully resolved, though we have found a set of boundary conditions which seem practical to use and yet do not radically change the nature of the solutions. The boundary conditions given in Appendices A and B are a possible alternative, and seem to give better results for the Holm-MHD equations. While our choice of boundary conditions was motivated by what we believe are sensible physical assumptions, we do not yet have a definite philosophy leading to a unique choice for the subgrid scale boundary conditions. This lack of a proper theoretical basis is a cause for concern, especially if we wish in the future to extend these ideas to different geometries. We must also not lose sight of the fact that the boundary layers play an important role in any strongly nonlinear convecting system, and hyperdiffusion can potentially have a big effect on the nature of these boundary layers. This alone means that hyperdiffusive solutions will need to be carefully interpreted before being applied to studies of the geomagnetic field.

It will also be of interest to see whether subgrid scale models such as the Holm-MHD model portray the small scale behaviour more faithfully than crude "eddy diffusivities" can do. In this study, the effects of the boundary layers have overwhelmed the effects of the modified nonlinear terms but, if the LANS α method can be adjusted to eliminate this difficulty, it may prove to be a fruitful research tool.

Acknowledgements. We thank the US National Science Foundation for support under grant EAR0222334, during the tenure of which this paper was written, and we also thank Darryl Holm for useful discussions.

References

Andrews, D.G. and McIntyre, M.E., "An exact theory of nonlinear waves on a Lagrangian–mean flow", *J. Fluid Mech.*, **89**, 609–646 (1978).

Andrews, D.G. and McIntyre, M.E., "On wave–action and its relatives", *J. Fluid Mech.*, **89**, 647–664. Corrigendum: *ibid*, **95**, 796 (1978).

Braginsky, S.I., "Magnetohydrodynamics of the Earth's core", *Geomagn. & Aeron.*, **4**, 698-712 (1964).

Braginsky, S.I. and Meytlis, V.P., "Local turbulence in the Earth's core", *Geophys. Astrophys. Fluid Dynam.*, **55**, 71–87 (1990).

Buffett, B.A., "A comparison of subgrid-scale models for large-eddy simulations of convection in the Earth's core", *Geophys. J. Int.*, **153**, 753–765 (2003).

Busse, F.H., "Convective flows in rapidly rotating spheres and their dynamo action", *Phys. Fluids*, **14**, 1301–1314 (2002).

Christensen, U., Olson, P. and Glatzmaier, G.A., " Numerical modelling of the geodynamo: a systematic parameter study", *Geophys. J. Int.*, **138**, 393–409 (1999).

Dormy, E., Valet, J-P. and Courtillot, V., "Numerical models of the geodynamo and observational constraints," *Geochem. Geophys. Geosyst.*, **1**, art. no. 2000GC000062 (2000).

Eckart, C., "Some transformations of the hydrodynamic equations," *Phys. Fluids*, **6**, 1037–1041 (1963).

Fearn, D.R., Roberts, P.H. and Soward, A.M., "Convection, stability and the dynamo", in *Energy, Stability and Convection* (eds G.P.Galdi and B. Straughan). Longmans, pp. 60–324 (1988).

Frick, P., Reshetnyak, M. and Sokoloff, D., "Combined grid-shell approach for convection in a rotating spherical layer", *Europhys. Lett.*, **59**, 212–217 (2002).

Gjaja, I. and Holm, D.D., "Self-consistent Hamiltonian dynamics of wave mean-flow interaction for a rotating stratified incompressible fluid", *Physica D*, **98**, 343–378 (1996).

Glatzmaier, G. A. and Roberts, P. H., "A 3-dimensional self-consistent computer simulation of a geomagnetic field reversal", *Nature*, **377**, 203–209 (1995).

Glatzmaier, G. A. and Roberts, P. H., "Simulating the geodynamo", *Contemp. Physics*, **38**, 269–288 (1997).

Grote, F.H., Busse, F.H. and Tilgner, A., "Effects of hyperdiffusivities on dynamo simulations", *Geophys. Res. Lett.*, **27**, 2001–2004 (2000).

Holm, D.D., "Averaged Lagrangians, and the mean effects of fluctuations in ideal fluid dynamics", *Physica D*, **170**, 253–286 (2002).

Jones, C.A. and Roberts, P.H. "Convection driven dynamos in a rotating plane layer", *J. Fluid Mech.*,**404**, 311–343 (2000).

Kono, M. and Roberts, P.H., "Recent geodynamo simulations and observations of the geomagnetic field", *Rev. Geophys.*, **40**, art. no. 1013 (2002).

Kuang, W. and Bloxham, J., "Numerical modeling of magnetohydrodynamic convection in a rapidly rotating spherical shell: weak and strong field dynamo action", *J. Comput. Phys.*, **153**, 51–81 (1999).

Montgomery, D.C. and Pouquet, A., "An alternative interpretation of the Holm "alpha model"," *Phys. Fluids*, **14**, 3365–3366 (2002).

Rotvig, J. and Jones, C.A., " Rotating convection-driven dynamos at low Ekman number", *Phys. Rev. E*, **66**, art. no. 056308, 1–15 (2002).

Soward, A.M., "A kinematic theory of large magnetic Reynolds number dynamos", *Phil. Trans. R. Soc. Lond., A***272**, 431–462 (1972).

Starchenko, S. and Jones, C.A., "Typical velocities and magnetic field strengths in planetary interiors", *Icarus*, **157**, 426–435 (2002).

Subramanian, K., "Hyperdiffusion in nonlinear large- and small-scale turbulent dynamos", *Phys. Rev. Lett.*, **90**, art. no. 90.245003 (2003).

Taylor, J.B. "The magneto-hydrodynamics of a rotating fluid and the Earth's dynamo problem", *Proc. R. Soc. Lond. A***274**, 274–283 (1963).

Walker, M.R., Barenghi, C.F. and Jones, C.A., "A note on dynamo action at asymptotically small Ekman number", *Geophys. Astrophys. Fluid Dynam.*, **88**, 261–275 (1998).

Zhang, K. and Jones, C.A., "The effect of hyperviscosity on geodynamo models", *Geophys. Res. Lett.*, **24**, 2869–2872 (1997).

Zhang, K., Jones, C.A. and Sarson, G.R., "The dynamical effects of hyperviscosity on numerical geodynamo models", *Stud. Geophys. Geodaet.*, **42**, 247–253 (1998).

Appendix A: Other magnetic boundary conditions

This appendix seeks an alternative to the boundary conditions (5.5) and (5.6) for the Holm-MHD equations, one that is better motivated from a physical point of view than (5.5) and (5.6). The basic idea is that the subgrid scale magnetic fields will penetrate from the conducting fluid into the surrounding insulator in the same way as the large scale fields do, and that therefore it is necessary to consider both filtered and unfiltered magnetic fields in the insulator. We shall distinguish these from the corresponding fields in the conductor by an added circumflex.

As in (4.10),

$$\widehat{g} = (1 - \alpha^2\nabla^2)\widehat{\overline{g}}, \qquad \widehat{h} = (1 - \alpha^2\nabla^2)\widehat{\overline{h}}. \tag{A1}$$

In the insulator, the unfiltered field is a source-free potential field, so that

$$\widehat{g} = 0, \qquad \nabla^2\widehat{h} = 0, \tag{A2}$$

and, by (A1),

$$0 = (1 - \alpha^2\nabla^2)\widehat{\overline{g}}, \qquad 0 = \nabla^2(1 - \alpha^2\nabla^2)\widehat{\overline{h}}. \tag{A3}$$

Since there are no sources of field at infinity, the relevant solutions of (A3) are those that vanish with distance from the conductor. It follows that, for the (l, m) components in $z \geq \frac{1}{2}$,

$$\widehat{\overline{g}}_{lm} = g_0 \mathrm{e}^{-nz}, \qquad \widehat{\overline{h}}_{lm} = h_0 \mathrm{e}^{-nz} + h_1 \mathrm{e}^{-az}, \tag{A4}$$

where, as before, $a = (l^2k_x^2 + m^2k_y^2)^{1/2}$ is the total wave number and $n = (a^2 + \alpha^{-2})^{1/2}$. [In (A4), g_0, h_0 and h_1 are constants.]

The conditions (3.19) and (3.20) on g an h follow from requiring that $\widehat{g} = g$, $\widehat{h} = h$ and $\widehat{h}' = h'$ on $z = \frac{1}{2}$. Similarly, $\overline{g}$, $\overline{h}$ and $\overline{h}'$ must be continuous there, so that (A4) requires

$$\partial_z\overline{g}_{lm} = \mp n\overline{g}_{lm}, \qquad (\pm\partial_z + a)\overline{h}_{lm} = -\alpha^2(n - a)\nabla^2\overline{h}_{lm} \quad \text{on} \quad z = \pm\tfrac{1}{2}. \tag{A5, A6}$$

(We have taken the opportunity here of including the conditions at $z = -\frac{1}{2}$ also.)

Conditions (A5) are supplemented by those obtained from (3.19), (3.20) and (4.10):

$$(1 - \alpha^2\nabla^2)\overline{g} = 0, \qquad (1 - \alpha^2\nabla^2)\overline{h}'_{lm} = \mp a(1 - \alpha^2\nabla^2)\overline{h}_{lm}, \quad \text{on} \quad z = \pm\tfrac{1}{2}. \tag{A7, A8}$$

Conditions (A6)–(A8) are the alternatives to (5.5) sought. One may also argue from (4.11) that the mean filtered field in the insulator must satisfy conditions similar to (A5):

$$\alpha\partial_z\bar{b}_x = \mp\bar{b}_x, \qquad \alpha\partial_z\bar{b}_y = \mp\bar{b}_y, \quad \text{on} \quad z = \pm\tfrac{1}{2}. \tag{A9, A10}$$

Appendix B: $\alpha-$layers

The relationship between $\mathbf{u}$ and $\overline{\mathbf{u}}$ in the Camassa-Holm approach is

$$\mathbf{u} = (1 - \Delta)\overline{\mathbf{u}}, \tag{B1}$$

where

$$\Delta = \nabla_i\overline{\xi_i\xi_j}\nabla_j. \tag{B2}$$

Their Taylor ansatz allowed them to assume that the correlation in the displacement $\boldsymbol{\xi}$ is homogeneous and isotropic:

$$\overline{\xi_i\xi_j} = \alpha_0^2\delta_{ij}, \qquad \text{where} \qquad \alpha_0 = \text{constant}; \tag{B3}$$

see (2.10). Then $\Delta = \alpha_0^2\nabla^2$ and (B1) reduces to (2.13).

At a fixed no-slip boundary, $\boldsymbol{\xi}$ is zero, and it is smaller than α_0 in an "$\alpha-$layer" adjacent to the boundary. Evidently $\overline{\xi_i\xi_j}$ increases with distance, z, from the boundary to become $\alpha_0^2\delta_{ij}$ as $z \to \infty$ on the boundary layer scale. This means that, as with every other situation in which there are reasons for

believing that $\overline{\xi_i\xi_j}$ is a function of position, $\boldsymbol{\nabla}\cdot\mathbf{u}$ and $\boldsymbol{\nabla}\cdot\overline{\mathbf{u}}$ cannot simultaneously be zero. The reason for this may be traced back to (2.8) which in general does not allow both $\overline{\mathbf{u}}$ and $\mathbf{u}'$ to be divergenceless. It seems clear that the unfiltered velocity must satisfy $\boldsymbol{\nabla}\cdot\mathbf{u}=0$ in the Boussinesq approximation, so that $\boldsymbol{\nabla}\cdot\overline{\mathbf{u}}\neq 0$ in the $\alpha-$layer, an unwelcome complication; it is not even possible to write $\overline{\mathbf{u}}$ in the form (3.5) in the $\alpha-$layer.

The thickness of the $\alpha-$layer is of order α_0 and, assuming that this is small compared with all other relevant length scales, the $\alpha-$layer is a type of surface layer abutting a locally flat boundary, $z=0$; moreover to leading order $\overline{\xi_i\xi_j}$ depends on z alone. In the generic case, $\boldsymbol{\xi}_H=\mathrm{O}(z)$ and $\xi_z=\mathrm{O}(z^2)$ as $z\to 0$, so that $\overline{\xi_{Hi}\xi_{Hj}}=\mathrm{O}(z^2)$, $\overline{\xi_{Hi}\xi_z}=\mathrm{O}(z^3)$ and $\overline{\xi_z^2}=\mathrm{O}(z^4)$. (Here the suffix $_H$ refers to 'horizontal', $x-$, $y-$components.)

The Camassa-Holm equations corresponding to (3.1) and (3.5) are, in the non-magnetic, non-buoyant case,

$$\hat{\mathbf{z}}\times\overline{\mathbf{u}}=-\boldsymbol{\nabla}p+E\nabla^2\mathbf{u},\qquad \boldsymbol{\nabla}\cdot\mathbf{u}=0, \tag{B4}$$

which, after the substitution (B1), are

$$\hat{\mathbf{z}}\times\overline{\mathbf{u}}+\boldsymbol{\nabla}p-E\nabla^2\overline{\mathbf{u}}=-E\nabla^2\Delta\overline{\mathbf{u}},\qquad \boldsymbol{\nabla}\cdot\overline{\mathbf{u}}=\boldsymbol{\nabla}\cdot\Delta\overline{\mathbf{u}}. \tag{B5, B6}$$

The $\alpha-$layer structure is determined by the $\mathrm{O}(\partial_z^3\,\overline{\alpha_z^2}\,\partial_z\overline{\mathbf{u}})$ part of the right-hand side of (B5), which shows that a singular solution exists that is of order $\exp(1/z)$ for $z\to 0$. The exclusion of this singularity places an implicit condition on each component of $\overline{\mathbf{u}}_H$. When the resulting two conditions are in force, the solution may be obtained conceptually by iteration. It is expanded as

$$\overline{\mathbf{u}}=\sum_{n=0}^{\infty}\alpha_0^{2n}\overline{\mathbf{u}}^{(n)}, \tag{B7}$$

substituted into (B5), and like powers of α_0^2 are equated. The resulting equations are each solved subject to no-slip boundary conditions.

Because the singular solution has been eliminated, the procedure just adumbrated succeeds both in the mainstream (i.e., outside the $\alpha-$layer) *and* within the $\alpha-$layer itself. Because $\boldsymbol{\nabla}\cdot\overline{\mathbf{u}}\neq 0$ in the $\alpha-$layer however, this is an inconvenient procedure to adopt in numerical work. Instead, the focus is best placed on the mainstream solution for which $\overline{\xi_i\xi_j}$ is constant. This requires boundary conditions to be applied at the "edge of the boundary layer" where $z=\mathrm{O}(\alpha_0)$ or, in the asymptotic sense, where $z\to 0$ on the mainstream scale but $z\to\infty$ on the boundary layer scale. Because $\alpha\neq 0$ at the edge of the boundary layer, 5 explicit conditions are required to replace the 2 implicit conditions and the 3 explicit conditions at $z=0$. Three explicit conditions at the edge of the boundary layer follow, via (B1), from the no-slip conditions on $\mathbf{u}$ at $z=0$; they are

$$(1+\alpha_0^2a^2)\overline{e}-\alpha_0^2\overline{e}''=(1+\alpha_0^2a^2)\overline{f}-\alpha_0^2\overline{f}''=(1+\alpha_0^2a^2)\overline{f}'-\alpha_0^2\overline{f}'''=0, \tag{B8}$$

where a is the total wavenumber defined in Appendix A.

The two further conditions would ideally express in mathematical terms the absence of the singular parts of $\overline{\mathbf{u}}_H$ in the $\alpha-$layer, but this idea is not easily implemented, and we have not completed the required analysis. We must therefore, as in Section 5, postulate two *ad hoc* conditions at the edge of the boundary layer. Even if transpires that these are not equivalent to the 2 implicit conditions, the resulting error will be mainly confined to a spurious boundary layer of thickness α_0 at the edge of the mainstream and will not be serious elsewhere. The simplest choice is $\overline{\mathbf{u}}_H=0$, i.e., $\overline{e}=\overline{f}'=0$. By (B8), the complete set of 5 conditions to apply at the edge of the boundary layer is then

$$\overline{e}=\overline{e}''=(1+\alpha_0^2a^2)\overline{f}-\alpha_0^2\overline{f}''=\overline{f}'=\overline{f}'''=0. \tag{B9}$$

For the x,y independent parts of the velocity field, the corresponding choice is

$$\bar{U}_x=\bar{U}_x''=\bar{U}_y=\bar{U}_y''=0. \tag{B10}$$